# Microcontact Printing Approaches to Pattern the Attachment of Endothelial Cells on Silicone Surfaces with Microgrooves

A Thesis

Submitted to the Faculty

of

Drexel University

by

Dheeraj Roy

in partial fulfillment of the

requirements for the degree

of

Master of Science in Biomedical Engineering

June 2010

## DEDICATIONS

*I dedicate this dissertation to Dr. Partha Sarathy Roy and Dr. Elizabeth Roy, my loving parents who always believed in me, no matter what.*

## ACKNOWLEDGEMENTS

I want to thank my family for their continued love and encouragement through these years. I also wish to thank my fiancé, Shruti Gour, for her affection and support through these trying times of my life. Thank you also for taking time out for meticulous proofreading and offering invaluable suggestions.

I am grateful to my thesis advisor, Prof. Kenneth Barbee, for his guidance and encouragement through my Master's studies. I had a chance to acquire a wealth of knowledge and skills while working with him.

I thank my thesis committee members: Dr. Peter Lelkes and Dr. Anat Katsir for their time and co-operation. Their constructive criticism and advice is greatly appreciated.

I would like to express my deep and sincere gratitude to my colleagues in the Cellular and Tissue Engineering Laboratory for their assistance and support. I express my appreciation to Ms. Allison Andrews for her guidance and assistance, which helped in moving this project forward. I thank Ms. Dannielle Figueroa for her assistance with microcontact printing. I am also thankful to Prof. Alisa Clyne for permitting me the use of the microfabrication facility in the Vascular Kinetics Laboratory.

# TABLE OF CONTENTS

# LIST OF TABLES

## LIST OF FIGURES

**ABSTRACT**

Microcontact printing approaches to pattern the attachment of endothelial cells on silicone surfaces with microgrooves

Dheeraj Roy

Advisor: Dr. Kenneth Barbee

Fluid shear stress (FSS) has been employed to create two-dimensional (2D) monolayers of endothelial cells (ECs) that resemble the organization of natural vasculature. However, shape-dependent EC properties that are independent of FSS remain largely undefined. More recently, surface micropatterning has been investigated as an approach to control the morphology and orientation of ECs using synthetic substratum. Most research studies have reported the effects of microtopography on sub-confluent layers of cells, which has been the standard in research investigations to date. In this thesis, surface micropatterning is used to mimic the natural EC vasculature in confluent layers of cells.

Cell alignment and elongation of bovine aortic endothelial cells (BAECs) were studied on poly(dimethylsiloxane) (PDMS) surfaces consisting microgrooves of parallel channels and ridges with depths of 100 nm, 500 nm, 1 µm, and 5 µm. The silicone surfaces were preadsorbed with 10 µg/ml fibronectin (FN), an ECM protein, to encourage cell attachment. More than 70% of the cells aligned in the 500 nm and 1 µm depth microgrooves as compared to the BAECs cultured on unpatterned substrates, which showed no preferential alignment. Further, the 1 µm depth resulted in maximum elongation (> 3.0) of BAECs using *Factor* E, which quantifies morphological differences

between cells on these microgrooves as compared to their counterparts on smooth silicone surfaces.

The effects of microtopography-induced alignment on the spatial localization of caveolae were investigated. Caveolae are microdomains of the plasma membrane that contain and regulate a variety of signaling molecules, and hence play an important role in cell function. Immunostaining protocols were employed to characterize spatial localization of the endothelial nitric oxide synthase (eNOS) and its primary regulatory protein, caveolin-1 (Cav-1). Analysis showed that the expression levels of eNOS and Cav-1 were significantly higher on 500 nm and 1 µm depth patterned surfaces. Based on the Mander's coefficient of colocalization, the 1 µm depth exhibited the highest percent colocalization (R=76%) of eNOS and Cav-1. These signaling molecules were observed to align within the channels of the 5 µm depth microgrooves, and similar alignment was observed for actin filaments. This indicates possible interactions between eNOS and Cav-1 with actin filaments. While PDMS microgrooves strongly influenced cell orientation and morphology, microcontact printing of fibronectin on smooth PDMS determined that these microgroove-based changes in cells are a result of the 2D surface geometry and the three-dimensional (3D) spatial arrangement of cells. In summary, PDMS substrates with patterned microgrooves provide a method for evaluating the interplay between cell orientation and spatial localization of membrane proteins, which may be patterned using microcontact printing techniques.

# 1. INTRODUCTION

The extracellular matrix (ECM) is made up of several proteins such as collagens, proteoglycans, and glycosaminoglycans, which provide a three-dimensional environment that organizes cells into tissues. The ECM contains topographical cues that are vital for *in vivo* cellular behavior such as cell attachment, migration, and proliferation (Zhu et al., 2004). The natural complexity of the ECM makes studies of cell behavior difficult, resulting in the need for an *in vitro* tissue culture model. Currently, most cell types in culture are plated on traditional two-dimensional (2D) dishes to be used for cell studies where cells are limited to the formation of a monolayer. This 2D model does not resemble the original organization of endothelial cells (ECs) in vasculature (Motlagh et al., 2003). Therefore, a cell culture system that provides a three-dimensional (3D) environment makes it possible to effectively study cellular processes in a physiological *in vitro* setting. Surface topography, utilizing micropatterning techniques, provides an approach to control the morphology and function of endothelial cells from native vascular vessels using a synthetic substratum (Vartanian et al., 2008).

An understanding of the effect of surface properties on cell behavior is important for designing substratum for controlling mammalian cell organization in basic and clinical research and in tissue- and cell-engineering applications. Poly(dimethylsiloxane) (PDMS) was chosen as the substrate to improve EC attachment due to its elasticity, ease of surface functionalization with ECM proteins and efficient processing. Chapter 2 consists of the

background information on a fluid shear stress (FSS) model for controlling EC shape, substratum topography-based cell behavior, and different topographic textures that have been shown to induce changes in cell orientation. A detailed list of the materials used and the procedures developed during the course of this thesis are given in Chapter 3. Chapter 4 shows the cell alignment and elongation of confluent bovine aortic endothelial cells (BAECs) on PDMS microgrooves with depths in the range of 100 nm – 1 µm. The 1 µm depth pattern resulted in maximum elongation of BAECs while maximum alignment was observed between 500 nm – 1 µm, thereby demonstrating the 1 µm as an ideal substrate to mimic *in vivo* vasculature. Also, the effects of cell alignment by microscale topography have been evaluated in terms of the colocalization of physiologically relevant protein markers. The 1 µm substrate resulted in maximum colocalization of endothelial nitric oxide synthase (eNOS) and Caveolin-1 (Cav-1), which are known to be important cell signaling proteins. Further, the effects of grooved patterns on BAECs have been obtained using microcontact printed (µCP) patterns of fibronectin that demonstrates the fact that changes in cell orientation are a result of the combination of 2D surface geometry and 3D spatial arrangement of cells. Finally, Chapter 5 discusses the role of actin filaments in regulating cell morphology in response to microtopography, and potential interactions of actin with signaling proteins such as eNOS and Cav-1. Therefore, the grooved topography is seen to provide a strong input for cell orientation, which may be obtained using 2D patterns of ECM proteins.

The specific aims of this project are identified are follows:

- Achieve cell alignment and elongation of confluent BAECs on PDMS surfaces containing microgrooves of varying depths.
- Demonstrate microcontact printing as an effective technique to determine whether changes in cell orientation are a result of the 2D surface geometry or a result of the 3D spatial arrangement of cells.
- Quantify the microtopography-induced alignment of BAECs on PDMS microgrooves and μCP patterns.
- Evaluate the effects of cell alignment by microscale topography on spatial localization of physiologically relevant protein markers.
- Discuss the role of actin filaments in BAEC alignment.

# 2. BACKGROUND

In this chapter, the biology of native vasculature and the important role of endothelial cells in regulating the structure and function of blood vessels will be discussed. Fluid shear stress (FSS) based in vitro models have been developed to create two-dimensional (2D) monolayers of endothelial cells (ECs) that more closely mimic in vivo organization, however, such methods are limited in the study of ECs. Surface micropatterning (MP) is a more recent technique that allows for the development of three-dimensional (3D) in vitro models to study the shape-dependent EC properties in the absence of FSS. Grooved topographic textures including pillars, waves, and fibers have been shown to induce changes in cell orientation and morphology in various cell types (Vartanian et al., 2008; Uttayarat, 2007). Such cell behavior has been attributed to mechanical stimuli that result in contact guidance-induced cellular alignment (Weiss, 1934). Further, the alignment of actin filaments has been identified as a possible explanation for the cell alignment and elongation observed on grooved substrates (Uttayarat, 2007). To gain insight into the mechanism responsible for micropattern-induced changed in cell morphology, the spatial localization of important signaling molecules must be considered. In addition to MP, microcontact printing (μCP) is an effective technique that creates cell orientation changes on 2D surfaces via protein boundaries, which may be useful in understanding the underlying mechanism of contact guidance.

## 2.1 Blood vessels and endothelial cells

The largest blood vessels, arteries and veins, have a thick wall of connective tissue and many layers of smooth muscle cells (SMCs). The wall is lined by a thin sheet of endothelial cells (ECs), or the endothelium, separated from the surrounding outer layers by a basal lamina. The amount of connective tissue and smooth muscle cells vary according to the vessel's diameter, but the endothelial lining is always present. In the finest vessels of the vasculature, the capillaries, the walls only consist of ECs and their associated basal lamina. Thus, it is clear that endothelial cells line the entire vascular system and control the passage of materials into and out of the bloodstream (Alberts et al., 2002).

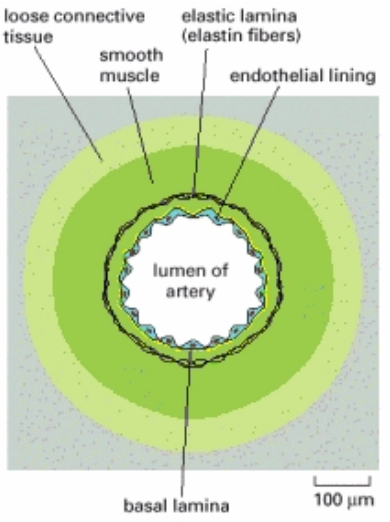


***Figure 1:*** *A small artery in cross-section showing the endothelial lining of blood vessels (Alberts et al., 2002).*

The endothelial lining provides a large surface area for the exchange of materials between blood and tissues (Baldwin and Thurston, 2001). The continuous monolayer of the endothelium if formed by cells linked to each other through different classes of cell-to-cell junctions (Michiels, 2003). Endothelial permeability changes are associated with redistribution of surface proteins, focal adhesions and activation of metalloproteinases. Loss of such barrier functions in pathophysiological conditions can cause extracellular edema and acute or chronic inflammation (Alexander and Elrod, 2002). Endothelial cells are important as a source of molecules that are involved in the regulation of blood coagulation and platelet function. Further, blood vessel damage results in the dominance of a procoagulant/prothrombotic phenotype of endothelial cells (Pearson, 1999).

Another crucial role of endothelial cells has to do with the maintenance of vascular tone. The endothelial cells release the free radical gas nitric oxide (NO), also known as the endothelium-derived relaxing factor (EDRF), which causes the relaxation of vascular smooth muscle cells (Palmer et al., 1987). The NO production by endothelial cells is enhanced by a variety of compounds, including acetylcholine, angiotensin II, and histamine. NO is synthesized from oxygen and L-arginine by endothelial NO synthase (eNOS), which have been reported to be activated via calcium pathways. With respect to the contraction of vascular smooth muscle cells, an endothelium-derived 21 amino acids peptide, endothelin (ET), is converted from its inactive state (proendothelin) to its mature state by endothelium membrane-bound metalloproteinases. The endothelin family of proteins exhibit vasoconstriction properties that are long lasting (Yanagisawa et al., 1988).

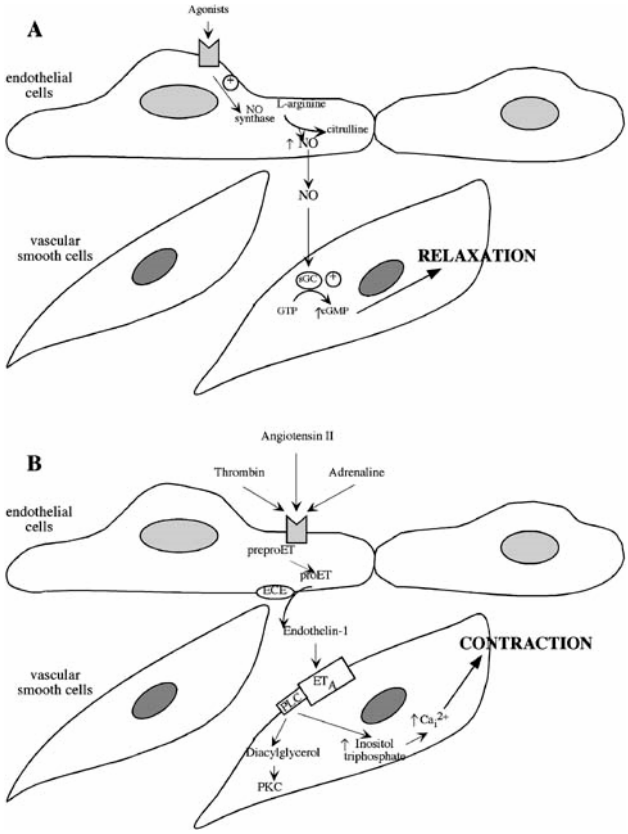


***Figure 2:*** *Schematic representation of the release of NO (A) and endothelin (B) by endothelial cells and their effects on smooth muscle cells, and consequently vascular tone regulation (Michiels, 2003).*

Therefore, endothelial cells are the main regulator of vascular homeostasis, acts as the interface between blood and tissue, and respond to changes in blood composition and blood flow. Disturbance of these parameters shift the endothelium from an antithrombotic, anti-inflammatory and vasodilating surface to conditions characterized by coagulation and vasoconstriction. A better understanding of endothelial cells will result in improved treatments for cardiovascular diseases and pharmacological strategies (Michiels, 2003).

## 2.2 Fluid shear stress and endothelial cells

In vivo increments in blood flow through arteries induces a vasodilation, which is abolished by the removal of endothelial cells, suggesting endothelium-dependent release of vasodilatory factors such as EDRF (Michiels, 2003). Increase in blood flow causes an increase in the hemodynamic forces on the vessel wall, specifically, shear stress, tangential forces acting in the direction of blood flow on the surface of endothelial cells, and pressure-stretch, which acts perpendicular to the vascular wall and affects endothelial cells and smooth muscle cells (Malek and Izumo, 1996). These forces result in morphological changes of endothelial cells, along with an array of biochemical changes, with the most profound being the increase in NO production with increasing shear stress. The latter has been associated to the rapid eNOS activation by shear stress and up-regulation of eNOS gene expression (Xiao et al., 1997).

Many studies have reported that shear stress induces a variety of acute and chronic changes of arterial structure and function in atherosclerotic vascular diseases (Fry, 1968). In 1986, Davies et al. showed that increasing shear stress resulted in the shift of endothelial cells with a polygonal shape at rest to oriented and elongated ECs in the direction of flow. This reorientation streamlined the endothelial cells, decreasing the effective resistance, which may be important in the adaptation of these cells to shear stress (Michiels, 2003). Since the discovery of this effect of shear stress on endothelial cells, many groups have focused their research on understanding the signaling mechanisms by which these monolayers detect changes in flow in the surrounding

environment and adapt their morphology accordingly. Shear stress has been implicated to promote the release of factors from ECs that inhibit coagulation, migration of leukocytes and smooth muscle proliferation, while simultaneously promoting endothelial cell survival (Chien et al., 1998).

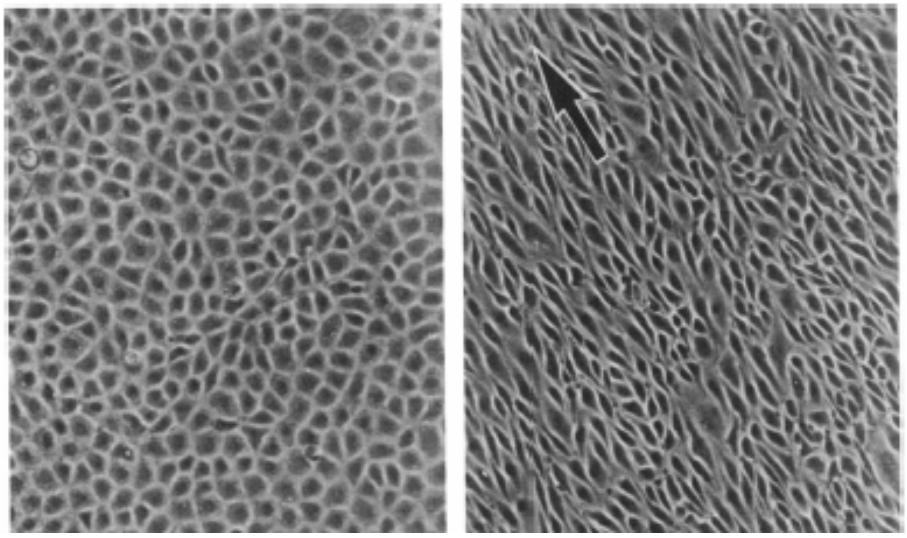

***Figure 3:*** *Monolayer of bovine aortic endothelial cells (BAECs) in static culture (left), and alignment of cells in a confluent monolayer after 24 hr exposure to 8 dynes/cm$^2$ (right) (Davies et al., 1986).*

Although fluid shear stress-based in vitro models have been developed to understand the mechanisms responsible for changes in endothelial cell morphology and function, shape-dependent endothelial properties that are independent of fluid shear stress remains largely undefined (Vartanian et al., 2008).

## 2.3 Surface microtopography

A more recent technique, surface micropatterning (MP), allows control of the cell shape independent of external forces, that is, using MP substrates, endothelial cell elongation and alignment can be achieved without the exposure to fluid shear stress (Vartanian et al., 2008). Surface MP is based on the concept of contact guidance first introduced by Weiss, which described changes in cell orientation as a response mechanism to the underlying topographic substrata (Weiss, 1934). Contact guidance has been observed in a variety of cell types, including neurons, fibroblasts, endothelial, epithelial, baby hamster kidney (BHK), Madin-Darby canine kidney (MDCK), macrophages, and neutrophils. In addition, contact guidance has been studied using a range of topographic structures, including grooves, pillars, waves and fibers (Uttayarat et al., 2005). Further, contact guidance has been reported to play a role in protein synthesis and growth in various cell types (Chesmel et al., 1995; Singhvi et al., 1994). Therefore, microtopography-based techniques allow the study the effects of endothelial cell shape on cellular and sub-cellular functions.

Many research groups have employed groove patterns consisting of ridges and channels to study the effects on cell orientation and elongation. These groove patterns were used to achieve strong alignment by varying the channel depth or the ridge width (Britland et al., 1996). The observations of these studies were consistent in the fact that maximum alignment resulted for ridge and groove widths narrower than the actual cell diameter (e.g. 10-20 µm for endothelial cells). One study was able to visualize uniformly

elongated bovine aortic endothelial cells (BAECs) using grooved PDMS substrates that were preadsorbed with an extracellular matrix protein (ECM), fibronectin, to improve adhesion of cells. Also, this study reported that focal adhesions aligned with the channel direction (Uttayarat et al., 2005). Similarly, another study used PDMS and poly(methyl methacrylate) (PMMA) nanogrooves to show significant elongation and alignment of bovine artery smooth muscle cells (SMCs), both in terms of the cell cytoskeleton and nuclei (Yim et al., 2005).

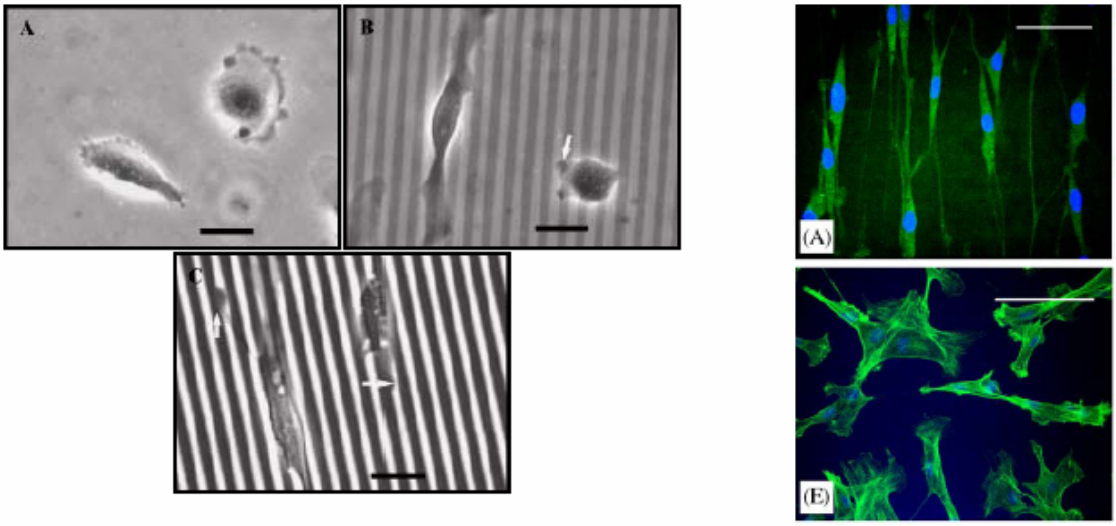


***Figure 4:*** *The set of images to the left (bar = 20 µm) are phase-contrast micrographs of BAECs on smooth (A), 200 nm (B), and 1 µm (C) PDMS after incubation for 1 h (Uttayarat et al., 2005). The set of images to the right (bar = 50 µm) are confocal micrographs of F-actin stained SMCs on patterned PMMA (A) and non-patterned PMMA (B) (Yim et al., 2005).*

The above images clearly demonstrate the usefulness of surface microtopography as a technique to mimic the uniformly elongated endothelium in natural linear blood vessels. However, most studies so far have focused on sub-confluent layers of cells rather than confluent monolayers. Therefore, it will be useful to apply surface micropatterning techniques to study topography-induced changes of confluent endothelial monolayers, which may help further understand the mechanisms involved in the detection of variations in the surrounding environment.

## 2.4 Mechanism of contact guidance

It has been widely accepted that cells receive chemical and physical signals from extracellular matrices, the surrounding fluid and from neighboring cells. Cells integrate the different stimuli and interpret them to generate appropriate cellular responses (Teixeira et al., 2003). Various cell types (previously mentioned) display contact guidance when cultured on groove and ridge patterns with lateral dimensions in the nanometer to micrometer range (Clark et al., 1990; Flemming et al., 1999). Significant differences in cytoskeletal organization have been found between cells elongated and aligned along topographic features and cells cultured on smooth surfaces. The complex network of the cytoskeleton, composed of actin filaments, microtubules, and intermediate filaments, have all been found to align along micrometer-sized grooves and ridges (Teixeira et al., 2003). On smooth substrates, cells and cytoskeletal components did not display any preferred orientations. In addition, focal adhesions, which are adhesive structures containing aggregates of transmembrane proteins called integrins that link the

actin cytoskeleton to extracellular matrix proteins, have been reported to preferentially align in the direction of grooves (Britland et al., 1996).

The sequence of cytoskeletal events and the relative importance of the actin and microtubule systems in the mechanism of contact guidance remain unclear. Oakley and Brunette proposed that the first event in the reaction of cells to grooves and ridges is the alignment of microtubules, approximately 20 minutes after cell plating (Oakley and Brunette, 1993). However, the detection of actin condensations along the groove/ridge boundaries 5 minutes after cell adhesion indicated that actin aggregation rather than microtubule alignment is the first event in the contact guidance mechanism (Wojciak-Stothard et al., 1995). On the other hand, one study used cytoskeletal poisons to disrupt either the microtubules or the microfilaments in cells cultured on micrometer-wide grooves and ridges, and still observed contact guidance (Walboomers et al., 2000). Comparing this to a study that investigated nanometer topographic features, found that functional microtubules are necessary for the initiation of contact guidance (Oakley et al., 1997).

Another explanation for contact guidance has been associated with focal adhesion formation and alignment, especially on submicrometer features since cell and cytoskeletal alignment has been more pronounced on patterns with ridge widths in the micrometer range (Matsuzaka et al., 2000). These adhesions have been found exclusively on the tops of ridges on narrower patterns and were aligned along these substrate features. In 2001, Riveline et al. proposed that focal adhesions orient along the direction

of the ridges to maximize their contact area, leading to an alignment of microfilament bundles and the cell body as a whole. However, several other studies have reported that focal adhesions bending along groove/ridge boundaries (Walboomers et al., 1998). Based on these hypotheses and explanations, it is clear that the mechanistic explanation of cell orientation by contact guidance requires further investigation.

## 2.5 Spatial localization of signaling molecules

To gain insight into the mechanism responsible for micropattern-induced changes in cell morphology, the spatial localization of important signaling molecules on smooth and patterned surfaces may be considered. Caveolin is a protein contained in discrete regions within the plasma membrane, where these discrete regions are commonly referred to as caveolae. Caveolin has been suggested to play an important role in regulating a variety of signaling processes. The physiological importance of caveolae is evidenced by recent studies reporting that caveolin deficiencies led to cardiovascular system abnormalities (Li et al., 2005). Caveolae formation on the cell membrane requires a cell surface plasma membrane protein, caveolin-1 or Cav-1. Caveolae and Cav-1 participate together in cellular processes such as vesicular transport, lipid metabolism, cholesterol homeostasis, and regulation of signal transduction (Cokakli et al., 2009). Hence, it is clear that Cav-1 plays an integral role in cell function.

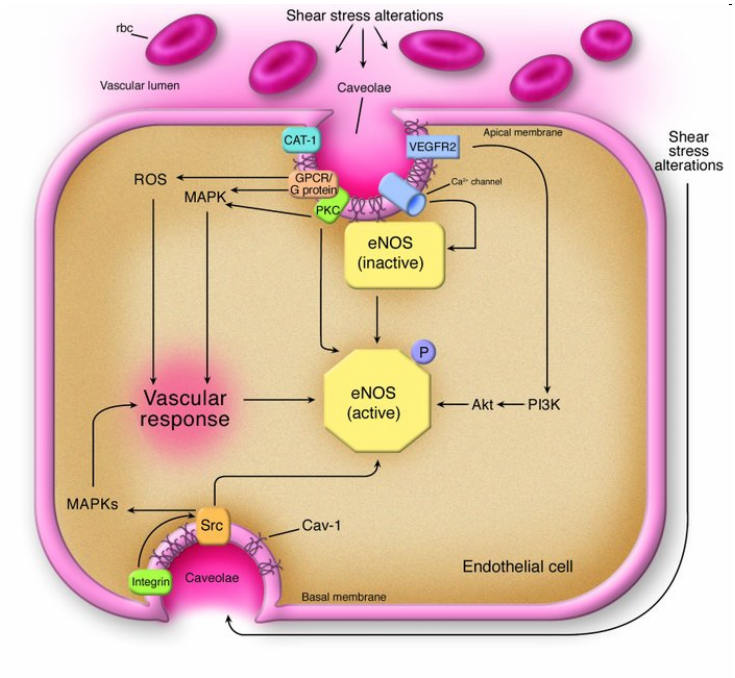


***Figure 5:*** *Caveolin-1 regulated signaling pathway in endothelial cells (Frank and Lisanti, 2006).*

Another important protein, endothelial nitric oxide synthase (eNOS), has been reported to control important cell processes such as angiogenesis, vasorelaxation, and permeability. eNOS is normally myristoylated and palmitoylated, which targets the protein to caveolae, where it resides in an inactive signaling complex due to association with Cav-1. Several studies have shown that caveolin-eNOS association leads to the inactivation of eNOS, thereby decreasing nitric oxide production (Li et al., 2005). This suggests that caveolae are involved in the temporal and spatial activation of eNOS. In addition, it has been reported that an increase in intracellular calcium results in a calmodulin-calcium complex displacing caveolin from eNOS, leading to enzyme activation (Ju et al., 1997; Cardena et

al., 1996). These findings confirm that caveolae and caveolin-1 are involved in eNOS regulation.

Considering that Cav-1 and eNOS are involved in important cellular processes, preliminary experiments should examine the changes in spatial localization of these proteins in endothelial cells plated on smooth, and microgrooved substrates made from PDMS. In addition, microtubules and actin microfilaments have been implicated in regulation of caveolae during their role in regulation of plasma membrane topography (Head et al., 2006). Furthermore, a study in 2007 by Ji et al. proposed that beta-actin plays a critical role in regulating nitric oxide production in platelets, which may be indicative of beta-actin interactions with eNOS. These findings suggest that actin microfilaments interact with caveolae during cell processes. In order to observe intracellular actin distribution, phalloidin, a drug that binds to actin filaments, may be utilized along with immunofluorescence microscopy (Wehland et al., 1977).

### 2.6 Microcontact printing to create topographical cues for cell patterning

PDMS substrates functionalized with micro- and nano-grooves provide a method for understanding the relationship between substrate topography and cell alignment. The drawback of using PDMS substrates lies in the fact that this method accounts for cell alignment and protein spatial localization resulting from groove width and periodicity (2D) as well as groove depth (3D). In order to determine cell orientation changes and protein expression levels resulting from 2D geometries or 3D depths, a quantitative

method is required that will allow for identification of the role of 2D and 3D cues, independently of each other. To address this limitation, microcontact printing (μCP) techniques may be employed for the extracellular matrix protein, fibronectin (FN), to identify the independent role of 3D cues in microtopography-induced cell alignment changes. Despite many reports on the effects of substrate topography on cells, the independent effect of 3D parameters on cell alignment has not been investigated (Choi et al., 2007).

Existing microcontact printing techniques include printing of peptides on poly(tetrafluoroethylene) surfaces using the ink-jet printer technology, protein-micropatterned lipid bilayer surface development using elastomer stamps and micropattern printing using lift-off techniques, microfluidic patterning and liquid-phase printing, micropatterning with photolithographic techniques, photolithography combined with plasma thin-film polymerization patterning, photoimmobilization generated patterns, and laser-guided patterning (Gauvreau et al., 2005; Kam and Boxer, 2000; Lim et al., 2007; Fiorini et al., 2005; Scotchford et al., 2003; Goessl et al., 2001; Herbert et al., 1997; Ashkin et al., 1987). Ink-jet technology, also known as jet patterning, has the advantages of being flexible with respect to substrate choice, inexpensive, and fast, while the spot size and resolution is limited by liquid/solid interfacial tension, printer resolution, and the nozzle diameter. Elastomer stamp-assisted patterning has advantages including that of not requiring specialized equipment once a master template is created, simple, large-scale and cost-effective. Additionally, two significant advantages of elastomer stamp-assisted technique are the suitability to virtually any substrate material,

and its potential use for immobilization of delicate molecules due to the absence of organic solvents. Limitations of stamp techniques is that the process is highly dependent on the mechanical properties of the stamping material and stamping of soft materials is still not entirely understood. Lift-off techniques enable an independent study of the influence of the cell-surface contact area and the ligand surface density, although, a major limitation of this technique is the inability to immobilize large proteins. Microfluidic patterning offers one of the easiest approaches to produce patterns consisting of many different molecules and provides improved control over surface-ligand density, while pattern geometries are limited to open network structures. Photolithography based techniques allow feature resolutions down to 1-2 µm, but a major drawback with this methodology is that the immobilized proteins are usually exposed to an organic solvent which may denature proteins to a certain degree. Photoimmobilization and laser-based patterning are capable of creating heterogeneous patterns by varying exposure time; however, these processes are slower as compared to other existing patterning methods (Falconnet et al., 2006).

A recent study used microcontact printing techniques to investigate the cytoskeletal structure of endothelial cells elongated on micropatterned surfaces to further their understanding of the relationship between cell shape, cytoskeletal organization, and cell function (Vartanian et al., 2008). The patterned surfaces consisted of 25 µm wide lanes of type I collagen with a spacing of 100 µm between lanes. The study reported complete endothelial cell alignment and elongation based on cytoskeletal organization on collagen patterns within 24 h. Further, the study showed that the alignment of EC actin fibers and

microtubules began almost immediately upon initial cell adhesion, while, FSS-induced actin elongation and alignment does not begin until 8-12 h after the onset of flow (Noria et al., 2004). Therefore, this study shows that microcontact printed patterns can isolate EC elongation and cytoskeletal alignment from FSS, and can be used to study the independent role of 2D cues on microtopography-induced alignment.

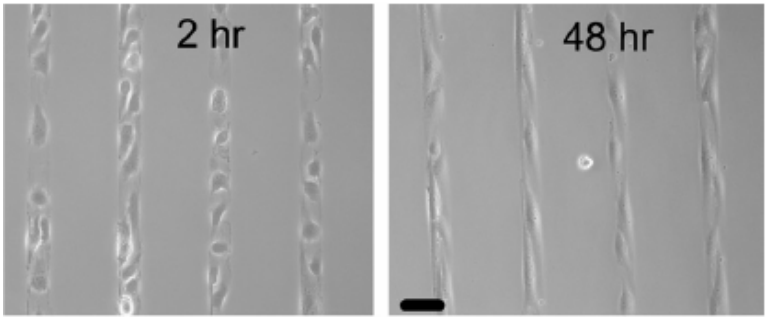


***Figure 6:*** *Baboon carotid artery endothelial cells on microcontact printed patterns of type I collagen showing the onset of alignment and elongation soon after initial adhesion (2 hr) as well as complete alignment (48 hr). The scale bar is 50 µm (Vartanian et al., 2008).*

Taking into consideration existing solutions to micropatterning, this research study will employ soft lithography techniques, specifically, microcontact printing (µCP). It is the most widely used among soft lithographic techniques due to its efficiency for producing substrates for cellular patterning (Singhvi et al., 1994). This technique will be employed

since it is very simple, cost-effective and flexible, with regards to the choice of substrate and the material (fibronectin or FN) to be transferred during printing.

# 3. MATERIALS AND METHODS

The microfabrication of the grooved substrates, the fabrication of elastomer stamps, the functionalization of substrates, the characterization, the experimental protocols, and the data analysis are described in this section. The materials required during the course of this thesis project have been detailed in section 3.1. The microfabrication of silicon molds film casting used to create grooved substrates, included photolithography and reactive ion etching (RIE) techniques, is described in section 3.2. Section 3.3 discusses the fabrication of elastomer stamps, sterilization and the protein printing, for microcontact printing of fibronectin. The immunostaining procedure for Cav-1, eNOS and actin filaments is outlined in section 3.4. The cellular distribution of proteins was assessed using three-dimensional (3D) surface plots of fluorescent images, which is discussed in section 3.5. Lastly, the data analysis methods for protein colocalization, cell orientation and cell elongation, are given in sections 3.6, 3.7 and 3.8 respectively.

## 3.1 Materials

Silicon wafers from Silicon Quest International (Santa Clara, CA), and negative resist, RD6 developer, and RR2 remover from Futurrex (Franklin, NJ). Sylgard 184 Silicone Elastomer kit to prepare cross linked PDMS from Robert McKeown Company, Inc (Branchburg, NJ). Fibronectin (FN) and Triton X-100 from Sigma (St. Louis, MO) and fluorescein isothiocyanate (FITC)-labeled phalloidin from Molecular Probes (Carlsbad,

CA). Primary anti-cav-1 and anti-eNOS polyclonal antibodies, as well as secondary Alexa, 4'-6-diamidino-2-phenylindole (DAPI), and Rhodamine (Rh) were purchased. Growth medium, serum, L-glutamine, penicillin, and streptomycin were purchased from Sigma-Aldrich. Para formaldehyde from Fisher (Newark, DE). Vectashield from Vector Laboratories (Burlingame, CA).

### 3.2 Microfabrication of grooved patterns

The grooved patterns of parallel ridges and channels were first created on silicon (Si) wafers using photolithography and reactive ion etching (RIE). A range of depths, i.e., 100 nm – 5 µm, were fabricated on the Si molds, after which they were used to create 3D groove patterns on PDMS substrates by the technique of film casting.

#### 3.2.1 Fabrication of silicon molds

Silicon (Si) molds were prepared to be used create grooved PDMS substrates. Photolithography and reactive ion etching (RIE) techniques were utilized to fabricate Si molds at the Microfabrication Facility, University of Pennsylvania. Si wafers were cleaned in deionized water-sulfuric acid mixture and dried with nitrogen gas. Negative resist was spun-coated onto Si, followed by UV exposure and drying under nitrogen. Photomasks were prepared by coating the resist-patterned wafers with Nichrome IV using an e-beam evaporation. Furthermore, RR2 solution was utilized to remove Nichrome IV-coated resist regions. These patterned Si wafers with Nichrome IV

photomasks were dry etched with RIE to create channels with depths of 100 nm, 500 nm, 1 µm, and 5 µm. After the RIE procedure, the photomask was removed, rinsed in deionized water and dried under nitrogen. These silicon molds were obtained from the Cellular and Tissue Engineering Laboratory.

***Table 1:*** *Channel and ridge widths for the respective depth of the grooved patterns (Uttayarat 2007).*

| Groove Depth | Channel Width | Ridge Width |
|---|---|---|
| 200 nm | 3.5 µm | 3.5 µm |
| 500 nm | 3.5 µm | 3.5 µm |
| 1 µm | 3.5 µm | 3.5 µm |
| 5 µm | 2.65 µm | 5.51 µm |

### 3.2.2 Film casting

Sylgard 184 Silicone Elastomer was utilized to cast the PDMS substrates. A mixture of curing agent to base resin in the ratio of 1:10 was poured onto grooved Si molds or a smooth Si wafer to create grooved or smooth substrates, respectively. The base resin was composed of 60 wt% dimethyl siloxane, dimethyl vinyl terminated, 30 wt% dimethylvinylated and trimethylated silica, 1-5 wt% tetra(trimethylsiloxy) silane and the cross-linker (or curing agent) was dimethyl methylhydrogen siloxane. The PDMS substrates were cured at room temperature (RT) for 48 h before experimentation. After

curing, the PDMS samples were annealed at 60ºC for 2 h to ensure complete cross-linking. For the cell orientation experiments, the PDMS samples were cut into squares using a sterile blade with approximate dimensions of 1 cm by 1 cm. Substrates were cleaned using 70% ethanol for 30 min to remove any residual monomer, then sterilized under ultraviolet (UV) light for one hour per side of the substrate and dried overnight in a tissue culture hood.

### 3.2.3 Substrate functionalization with fibronectin

Smooth and grooved PDMS substrates were immersed in a 10 µg/mL FN in phosphate buffered saline (PBS) solution at room temperature. This concentration of FN has been reported to produce monolayer coverage on hydrophobic surfaces (Uttayarat et al., 2005). Adsorption times were 1 h for smooth PDMS and 3 h for 100 nm and 500 nm PDMS, while it was increased to 5 h for 1 µm and 5 µm PDMS microgrooves. The time was increased for the micrometer-depth grooved substrates to ensure monolayer coverage of FN.

### 3.2.4 Cell culture

BAECs were cultured in T75 flasks using Dulbecco's Modification of Eagle's Medium (DMEM) supplemented with 10% fetal bovine serum (FBS), 0.5 mg/mL L-glutamine, 10 U/mL penicillin, and 10 µg/mL streptomycin at 37°C in 95% air/5% $CO_2$. Cells were sub-cultured every 2 days and cells at passages 8-24 were used for experimentation.

BAECs were seeded onto PDMS samples at a density of 50,000 cells/cm$^2$ in DMEM containing 10% FBS. For cell orientation experiments, cells on substrates were incubated for 24-36 h, and cell culture media was changed every day for culture times' greater (≥) than 24 h. The differences in passage numbers did not affect the outcome of the cell alignment, elongation and protein colocalization studies.

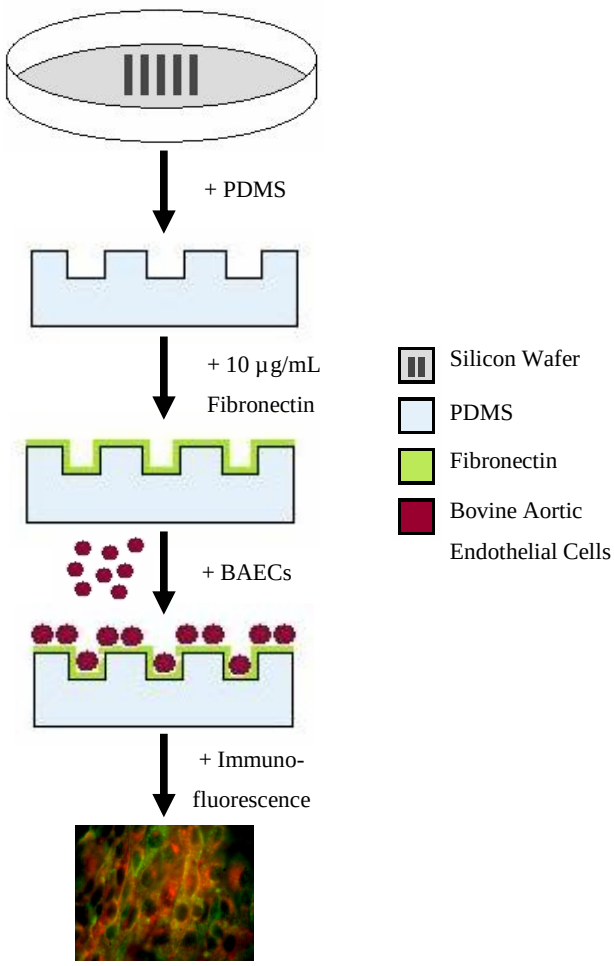


***Figure 7:*** *Block diagram representation of PDMS microgroove experiments.*

### 3.3 Microcontact printing

To evaluate the effects of two-dimensional (2D) surface geometry on cell orientation and compare the results to the 3D PDMS microgroove experiments, microcontact printing of fibronectin on smooth PDMS substrates was performed. In these experiments, the alternating channel and ridge pattern of the PDMS microgrooves was recreated by printing parallel patterns of FN using an elastomeric stamp. The stamps were prepared by film casting of PDMS on Si patterns (200 µm channels and 50 µm ridges) provided by the Vascular Kinetics Laboratory in the Mechanical Engineering Department at Drexel University. Since 2D surface geometry was being analyzed, the depth of the Si molds was not an important consideration. After successful fabrication of the elastomeric stamps, sterilization and FN surface functionalization was done, after which the printing of FN on smooth PDMS was performed. This resulted in 2D patterns of FN that mimicked the 3D patterns of parallel ridges and channels. After protein printing, the patterns were cultured with BAECs that were fluorescently labeled for important signaling molecules.

#### 3.3.1 Fabrication of elastomeric stamps

Two Si molds with patterns of parallel channels and ridges were used, one with a channel and ridge width of 200 µm and 50 µm respectively, and the other with a channel and ridge width of 10 µm. The elastomeric stamps were fabricated by film casting of Sylgard 184 Silicone Elastomer. Similar to the PDMS microgroove fabrication, a mixture of 1:10 curing agent to base resin was poured onto grooved Si molds or a 3 µm diameter Si wafer

to create the elastomeric stamps or smooth substrates for printing, respectively. The stamps were cut in squares of side 1 cm. The PDMS stamps were cured at room temperature for 48 h before experimentation, followed by cleaning using 70% ethanol and UV sterilization.

### 3.3.2 Printing patterns of fibronectin

To start the microcontact printing procedure, the elastomeric stamps were washed with 70% ethanol and dried using compressed nitrogen ($N_2$), washed with deionized (DI) water and air dried for 30 min at room temperature. After the incubation at room temperature, the stamps were baked in an oven for 10 min at 50ºC to ensure complete drying of the stamp surface has been achieved. With the dry stamps, 100-200 µL of 10 µg/mL fibronectin was added on the grooved surface of the stamps. This concentration of FN was used to remain consistent with the FN functionalization performed for the PDMS microgroove experiments. The stamps with FN were incubated for 1 h at 37ºC to achieve successful adhesion of protein to the stamp surface.

During the stamp-FN incubation, the smooth PDMS substrates were cut into 2 cm by 2 cm squares using a sterile blade. In order to successfully transfer protein from the hydrophobic elastomeric stamp to the smooth PDMS substrates, a hydrophobic-hydrophilic interaction had to be created. This was achieved by oxygen ($O_2$) plasma treating the smooth PDMS substrates that had a hydrophobic surface, which resulted in a hydrophilic surface on the smooth substrates. Since PDMS is a hydrophobic material, it

has been shown that oxygen plasma treatment under pressure can change the surface property of PDMS to hydrophilic, which is based on the principle of diffusion (Mokkapati et al., 2001). Therefore, the smooth PDMS substrates were oxygen plasma treated for 30 sec before the actual printing process was performed.

Following the stamp-FN incubation, the stamps were gently dried using Kim wipes and compressed nitrogen gas. The stamps were inverted on to the plasma treated smooth PDMS substrates and incubated at 37ºC for 30, 60, 90, 120, 150, and 180 min. The optimal incubation period for complete FN transfer from the elastomeric stamp to the smooth substrates was determined as 180 min. Therefore, for the cell orientation and immunostaining experiments, the stamp-substrate sandwiches were incubated for 180 min. It was important to compare different incubation times since the optimal incubation time varies with the protein being printed. Following this incubation, the printed substrates were washed with DI water, dried, and stored at 4ºC. To confirm successfully printing, the printed substrates were imaged under a light microscope using a 10x objective.

### 3.3.3 Sample preparation and cell culture

For cell orientation and immunostaining experiments using the microcontact printed PDMS substrates, following the printing and washes with DI water, the substrates were incubated at room temperature in PBS for 5 min (2x). After the PBS washes, the printed FN patterns were blocked using 0.2% Pluronic, which coated the non-protein printed

areas of the substrate and prevented non-specific cell attachment. Specifically, Pluronic is a non-ionic triblock copolymer composed of a central hydrophobic chain of polyoxypropylene flanked by two hydrophilic chains of polyoxyethylene. In these experiments, the substrates were incubated in Pluronic F-127 for 60 min at 37ºC followed by rinsing of the substrates with PBS for 5 min each that removed any residual Pluronic. After completing the sample preparation for the printed substrates, they were stored at room temperature in PBS until the BAECs were cultured from T75 flasks using DMEM. Similar to the PDMS microgroove experiments, passages 8-24 were used for microcontact printing experiments. Cells were seeded onto the FN patterns at a density of 50,000 cells/$cm^2$ and incubated for 1 h at 37°C to ensure cell adhesion to the substrates. After 1 h, the substrates were washed with DMEM to remove cells that were not attached to the surface, and fresh media was added for the overnight incubation at 37°C in 95% air/5% $CO_2$.

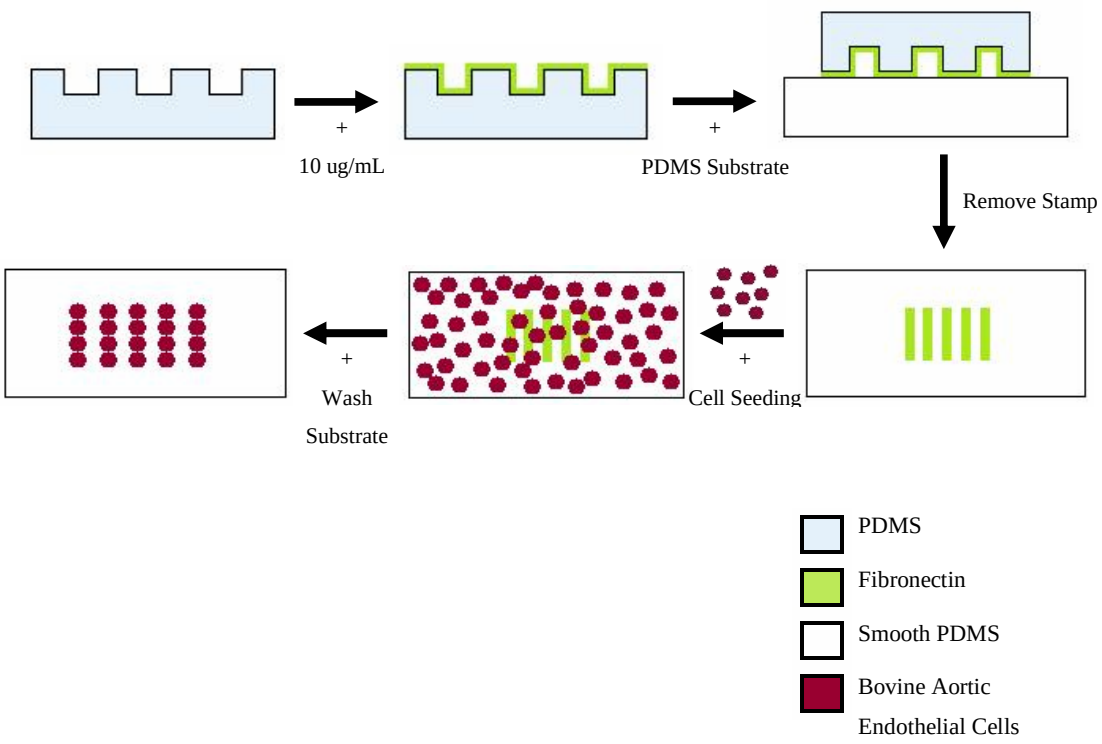


***Figure 8:*** *Block diagram representation of the microcontact printing experiments.*

### 3.4 Immunostaining of signaling proteins, Cav-1 and eNOS, and actin filaments

The spatial localization of Cav-1 and eNOS, proteins involved in the regulation of signaling pathways in endothelial cells, as well as the organization of actin filaments were visualized by immunofluorescence. For fluorescent imaging of regulatory proteins and actin filaments, a Leica DMRX microscope was used that is available at the Cellular and Tissue Biomechanics Laboratory.

### 3.4.1 Regulatory signaling proteins: Cav-1 and eNOS

For quantitative image analysis, the PDMS samples were first washed twice with PBS to remove non-adherent cells. Adherent cells were fixed in 4% paraformaldehyde (PFA) for 20 min at room temperature, followed by three washes with PBS. Cells were permeabilized in 0.1% Triton X-100 for 10 min at room temperature, followed by three washes with PBS. The nonspecific antigenic sites were blocked in 10% donkey serum (DKS) for 30 min at room temperature, followed by three washes with PBS. All primary and secondary antibodies were diluted in PBS. Following incubation at room temperature for 60 min in 1:200 mouse anti-eNOS and 1:200 rabbit anti-cav-1, samples were washed three times with PBS, and then incubated in the dark, at room temperature for 45 min in 1:500 donkey anti-rabbit Alexa 488 and 1:100 donkey anti-mouse IgG conjugated to Rhodamine Red-X. After 45 min, samples were washed three times with PBS, approximately 25 µL of Vectashield was added to each sample, and samples were covered with a glass cover slip. Samples were examined by phase contrast and fluorescence microscopy.

### 3.4.2 Actin filaments

Similar to the Cav-1 and eNOS imaging sample prep, the PDMS samples for actin imaging were rinsed with PBS and adherent cells were fixed in 4% PFA. Excess aldehyde was quenched in 0.1 M glycine for 5 min at room temperature, followed by three washes with PBS. Cells were permeabilized in 0.1% Triton X-100 for 20 min at

room temperature, followed by three washes with PBS. The staining solution was diluted in PBS. Samples were incubated in the dark, at room temperature for 30 min in 1:2 Phalloidin conjugated to fluorescein (FITC). After 30 min, samples were washed three times with PBS and covered with a glass cover slip. Samples were examined by phase contrast and fluorescence microscopy.

### 3.5 Cellular distribution of proteins

To observe differences in the spatial localization of Cav-1 and eNOS on microgrooves as compared to smooth substrates, as well as differences on microcontact printed patterns, the Java-based image processing program, ImageJ, developed at the National Institutes of Health (NIH, Bethesda, MD) was employed. Cellular distribution was analyzed using fluorescent images and an ImageJ plug-in '3D Surface Plot' (created by Kai Uwe Barthel, University of Applied Sciences, Berlin, Germany). This plug-in allows for the creation of 3D surface plots from 2D fluorescent images, which was useful in comparing the cellular distribution of proteins between samples. The luminance of each pixel in the fluorescent image is interpreted as the height for the plot. The plot display color scheme was selected as the fire LUT since it enhanced small differences between experimental and control images. Another advantage of using this plug-in is the fact that scale, rotation, perspective and position were adjustable. In this project, the individual cells were cropped and visualized in 3D, after which the most optimal scale and perspective was determined. These small differences were further enhanced by adjusting the lighting option, which improved visibility of minor details in the 3D plots. In addition, among the

different drawing modes, the filled mode was selected since the entire surface of the cells needed to be analyzed. However, there was one important consideration in order to accurately compare cells using these 3D surface plots, and that was related to the fact that the pixel luminance of fluorescent images was interpreted as the height, which implied that the software was highly sensitive to background. Therefore, to overcome this limitation, a background subtraction was performed on all fluorescent images prior to the application of the 3D plotting program using the free software by Olympus Microscopes (Background Subtraction Toolkit).

### 3.6 Cell characterization: orientation and elongation

To cells on PDMS microgrooves, microcontact printed patterns and smooth substrates were characterized with respect to their orientation and elongation. Quantification of cell orientation was based on the angle of cells with respect to the groove direction determined using the free open-source software, CellProfiler (Carpenter et al., 2006). To specifically outline cells in fluorescent images, ImageJ was used to adjust brightness and contrast of the original images so that the CellProfiler program (MATLAB interface) would be able to successfully identify the cell borders. In certain cases, the cells were manually selected for the CellProfiler analysis. Once the cells were outlined accurately, the major and minor axes were defined by the long direction of the cell body and the direction perpendicular to the major axes, respectively. For cell orientation, the angle between the major axes and the groove direction was used. Such a definition of major and minor axes resulted in both, thinner and longer cells as well as wider and shorter cells, to

be approximated as an ellipse. In the case of rounder cells, this ellipse approximation was not able to completely include the entire surface of the cell. The elliptical approximations for the two populations of cells (long and narrow versus circular and wide) are seen in the figure below.

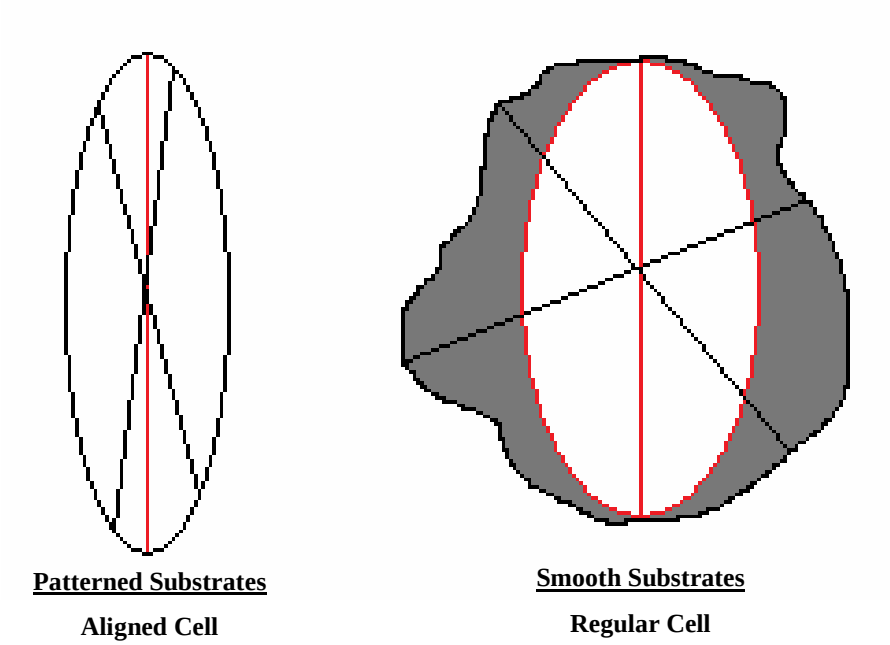


***Figure 9:*** *Visual representation of the ellipse approximations performed using the CellProfiler software to quantify cell orientation and elongation.*

For smooth substrates, cell orientation was defined relative to arbitrary axes defined as north-south (N-S) because these surfaces lacked an internal direction. To compare the orientation between grooved patterns of different depths, cells were considered aligned if

the angle between the long axis and the groove was less than 15º (Yim et al., 2005). Based on this definition, the percentage cell alignment was calculated for 30-40 cells.

To compare cell morphology on patterned and smooth substrates, an elongation index, Factor E, was calculated using the major and minor axes of the ellipse approximations (Yim et al., 2005). The elongation parameter (E) describes the extent the equimomental ellipse is lengthened or stretched out (Andersson et al., 2003). The E is zero for a circle, and one for an ellipse with an axis ratio of 1:2.

**Factor E = (long axis / short axis) - 1**

(Equation 1)

Where,

-Factor E represents the elongation index of the cell, or a parameter that shows differences in morphology.

-Long axis or the major axis is the longest axis that fit within the ellipse approximation.

-Short axis or the minor axis is the axis perpendicular to the longest axes based on the ellipse approximation.

The factor E was measured for 30-40 cells for grooved and smooth substrates. In addition, statistical analysis was performed on cell orientation and elongation, which is discussed in section 3.6.1.

### 3.6.1 Statistical analysis

All values were reported as the mean ± standard deviation (SD), where n = 30 to 40 for orientation and elongation experiments. The statistical significance of the differences between experimental groups was determined using the Student's *t*-test. Significance level was set at $p < 0.05$. Furthermore, to compare the population distribution of cell orientation between grooved or FN printed patterns and smooth substrates, the Kolmogorov-Smirnov test (K-S test) of statistical significance was performed. The K-S test is a nonparametric test that quantifies the distance between the empirical distribution functions of two samples. The advantage of this test is that it is insensitive to the shape of the distributions, and is only based on the relative distributions. To compare differences between samples, the D-statistic of the K-S test, which represents the maximum difference between cumulative distributions, was calculated. This statistic was used to compute the probability value. For the K-S test, the level of significance was set at 5%.

## 3.7 Protein colocalization analysis

To quantify the spatial localization of two proteins, Cav-1 and eNOS, that have been labeled using fluorescent immunocytochemistry, a colocalization analysis was performed. The method used in this thesis is known as the Mander's Coefficient (R) of colocalization (Manders et al., 1993). The value of the coefficient ranges between 1 and 0, with 1 being high-colocalization and zero being low. This method was determined applicable for this project since a requirement of the Mander's Coefficient is that the number of objects in

both channels of the fluorescent image be more or less equal. An important advantage of the Mander's Coefficient is the simplicity of interpreting the coefficient with respect to colocalization of proteins, as compared to other quantitative methods such as the Pearson's Correlation Coefficient, which ranges from -1 to 1 and is difficult to interpret for fluorescent images. The Mander's Coefficient for two channels, red and green, is expressed as:

$$R = \frac{\sum_i (R_i \times G_i)}{\sqrt{\sum_i (R_i)^2 \times \sum_i (G_i)^2}}$$

(Equation 2)

Where,

R represents the Mander's Coefficient of colocalization.

i represents the pixel number in the images.

$R_i$ is the intensity of the red channel.

$G_i$ is the intensity of the green channel.

A limitation of most colocalization coefficients is their sensitivity to background, and the same is true for the Mander's Coefficient. A properly acquired image has a certain amount of background to make sure that the 'real signal' that is above the background is detected. If this non-zero background is not removed, the quantification algorithms

assume it represents red or green signal, and assigns it a positive correlation value. To address the issue of background sensitivity, the threshold of the fluorescent images were determined using the ImageJ software, which was followed by a background subtraction. The threshold calculation using ImageJ reports a value of the mean background + 3x the standard deviation of the background.

Along with the calculation of the Mander's Coefficient, the relationship between the red and green pixels in an image is displayed as an intensity-scatter plot to obtain information regarding the frequency of the red-green pixel combination as well as the actual pixel colors in an image. For the latter, two scatter plots are created, one known as the 'Frequency plot', and the other is the 'Red-Green scatter plot'. In each scatter plot, typically the red image component is represented along the x-axis while the green image component is represented along the y-axis. The intensity of a pixel in the red image is used as the x-coordinate of the scatter plot and the intensity of the corresponding pixel in the green image as the y-coordinate. The 'Frequency plots' show pixels that is pseudocolored so that their color represents the frequency of the red-green pixel combination in the original image, while the 'Red-Green scatter plots' represent the pixels as the actual colors in the image. Therefore, the first type of scatter plot contains the most information but is difficult to relate back to the original image, and the second type of scatter plot is easier to relate to the original image but does not give any information about frequency.

A third parameter that is considered with the Mander's Coefficient of colocalization is referred to as the intensity correlation quotient (ICQ). The ICQ plots of both channels in the image, red and green, are compared to determine whether the red and green pixel intensities vary in synchrony (i.e., they are dependent), or vary asynchronously. If the red and green channel pixel intensities vary asynchronously, it indicates that the overlapped pixels are largely randomly associated, which does not depend on the Mander's Coefficient of colocalization. These plots consist of the product of the differences from the mean (PDM) on the x-axis with pixel intensity on the y-axis. Based on the Mander's Coefficient of colocalization, the intensity scatter plots, and the ICQ plots, it is possible to accurately compare the colocalization of Cav-1 and eNOS between grooved and smooth substrates. The statistical analysis of the percentage colocalization is presented in section 3.7.1.

### 3.7.1 Statistical analysis

All values were reported as the mean ± standard deviation (SD), where n = 30 to 40 for protein colocalization experiments. The statistical significance of the differences between experimental groups was determined using the Student's *t*-test. Significance level was set at $p < 0.05$.

# 4. RESULTS AND DISCUSSION

## 4.1 Microgroove surface topography regulates cell orientation

Recent studies have shown that cell shape in two-dimensional and three-dimensional tissues are closely related to functional aspects of cells, including proliferation, migration, differentiation, metastasis, and gene expression (Folkman and Moscona, 1978). Shaping of cells in living tissues is determined either by an organized extracellular microenvironment, specifically the extracellular matrices (ECM), or by a dynamic mechanical environment such as fluid shear stress. It is widely known that physiological stress induces various cellular responses through signaling pathways that affect cell orientation; however the underlying mechanisms have not been elucidated. The use of microgroove surface topographies (as described in section 3.2) provides a method to study cell shape under static conditions, which have been shown to affect intracellular structures including cytoskeletons, protein expression, signaling pathways, and cellular functions (Kato et al., 2001).

Most surface topographies used to study cell behavior were at micron dimension. Studies have shown that cells are more sensitive to their environment because they can ‘sense’ objects as small as 5 nm (Curtis and Wilkinson, 2001). Also, research has found that groove depth is most important in determining cell orientation (Zhu et al., 2004). Therefore, the objective of this study is to optimize the depth of groove patterns, made of

parallel ridges and channels, using poly(dimethylsiloxane) (PDMS) that will result in bovine aortic endothelial cells (BAECs) emulating the naturally aligned endothelium of the vascular vessels. The groove depth was varied from a nano- to a micro-scale, specifically 100 nm, 500 nm, 1 µm, and 5 µm, to account for the different mechanical cues that may be involved in shaping of cells in vivo. The grooved surfaces were preadsorbed with a uniform coverage of fibronectin (FN) so that differences in cell alignment and protein localization could be attributed to the variation in the groove depth. For the 100 nm – 1 µm patterns, the ridge and channel widths were held constant at 3.5 µm, while the 5 µm pattern exhibited a channel width of 2.65 µm and a ridge width of 5.51 µm. These patterns were cultured with BAECs and stained for important signaling proteins, Cav-1 and eNOS, to investigate cell orientation, cell elongation, and cell morphology. Further, these patterns were used to study the cellular distribution of Cav-1 and eNOS as well as the percentage colocalization, which are discussed in the following sections.

The results showed that increasing the groove depth from 100 nm to 1 µm resulted in an increase in cell alignment, where cells were considered aligned if the angle between the long axis of the cells and the grooves was less than 15º. In terms of morphology, aligned cells depicted an elliptical shape while cells on smooth substrates showed a circular shape. Further, the 1 µm pattern showed cells with an elongation parameter, *Factor* E, which was significantly greater compared to the other patterns. Along with shape changes, it was observed that protein colocalization showed a significant increase on the 1 µm pattern, which may be related to the elongation of cells on this groove depth.

### 4.1.1 PDMS substrate characterization and fibronectin adsorption

The smooth and grooved substrates were inspected for quality purposes using the atomic force microscope (AFM) and scanning electron microscope (SEM) by the Cellular and Tissue Engineering Laboratory. Briefly, the grooved substrates with depths of 100 nm, 500 nm, 1 µm, and 5 µm exhibited a pitch of 8 µm. The channel and ridge dimensions for each individual groove pattern can be found in section 3.2.1 (Table 1). The characterization results are detailed in Uttayarat et al. (2005).

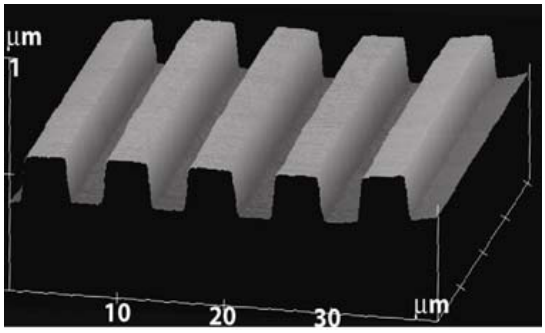


***Figure 10:*** *AFM image showing the cross-sectional profile of grooves on the PDMS mold with a groove depth of 200 nm (Uttayarat, 2007).*

As for the fibronectin adsorption performed in this research study, the procedure closely followed published protocols, which resulted in an average fibronectin surface density of 300-350 ng/cm$^2$ based on relative fluorescence intensities. In addition, this surface density value was reported to be identical among smooth and grooved PDMS substrates

(Uttayarat et al., 2005). Based on these results, it is clear that the smooth and grooved substrates were covered with a uniform layer of fibronectin, which allows differences in cell orientation and protein localization between substrates to be attributed to variations in groove depth rather than surface chemistry.

### 4.1.2 Endothelial cell shape: orientation, elongation and morphology

In this study, BAECs cultured on 200 nm – 5 µm groove depth PDMS patterns were quantified with respect to cell orientation relative to the groove direction and the cell elongation index (*Factor* E). These parameters were selected since they have been the most commonly used quantification methods to describe cell shape in published studies. This allows for a discussion to determine whether any relationships between cell shape and microtopography observed in this study is comparable to other studies. In addition to orientation and elongation, cell morphology was compared between substrates.

To visualize BAECs on PDMS substrates, the cells were fluorescently labeled using antibodies that recognized two regulatory signaling proteins, Caveolin-1 (Cav-1; green channel) and endothelial nitric oxide synthase (eNOS; red channel) (Figure 11). The grooved patterns were prepared by film casting PDMS on the surface of the silicon wafers. Since each pattern was on an individual 3 µm Si wafer, the PDMS groove surfaces were compared to their respective smooth regions on the same PDMS mold. This was done to compare consistency of the control samples across different Si wafers,

and to take into consideration any minor differences in surface properties of the individual Si wafers.

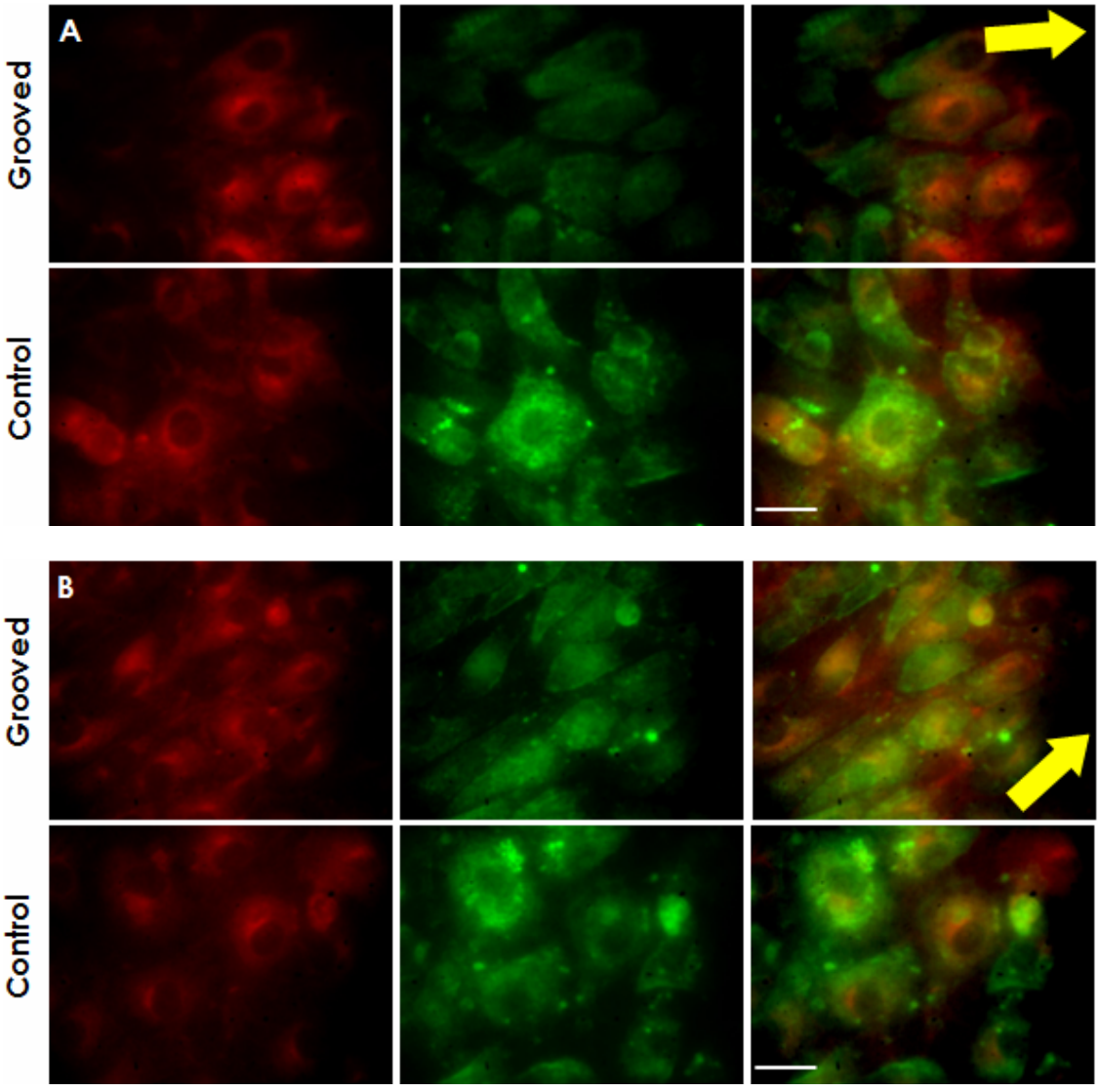


***Figure 11:*** *Fluorescent microscopy images of BAECs on both, grooved and smooth surfaces, for channel depths of 200 nm (A) and 500 nm (B). eNOS (red), Cav-1 (green) and merged channels show protein distribution. The scale bar is 25 µm.*

Figure 11 (above) shows the effects of nanoscale groove depths (200-500 nm) on BAEC orientation and elongation. The yellow arrows represent the groove direction for their respective groove depths. For the 200 nm groove depth, it is observed that some cells tend to orient in the direction of the grooves, while others exhibit random orientations that are similar to the cells on the control (smooth) surfaces (Figure 11A). In terms of elongation and protein expression levels, the cells on the patterned surfaces do not show significant differences as compared to their counterparts on the smooth substrates. On the other hand, BAECs on the 500 nm pattern show a majority of cells aligned in the direction of the grooves, which is significantly different (visually) compared to the controls (Figure 11B). In addition, levels of eNOS appear slightly increased in the grooved sample while those of Cav-1 are similar to the non-aligned cells. Comparing the results of the nanoscale groove depths, it is clear that increasing the depth from 200 nm to 500 nm caused an increase in the number of cells aligning in the direction of the grooves. In terms of morphology, the 500 nm groove cells show approximate elliptical shape while the 200 nm groove shows a combination of circular and elliptical shaped cells.

After making some observations about nanoscale grooves and their effects on cell orientation, it is important to consider micron-sized grooves as shown in Figure 12. Specifically, the figure shows BAECs cultured on 1 µm and 5 µm channel depth groove patterns that were subsequently visualized using immunostaining. The 1 µm groove pattern shows an entire confluent monolayer of BAECs aligning parallel to the groove direction (Figure 12A). In addition, significant differences are observed in the protein expression levels of eNOS and Cav-1 between the pattern and the smooth substrates.

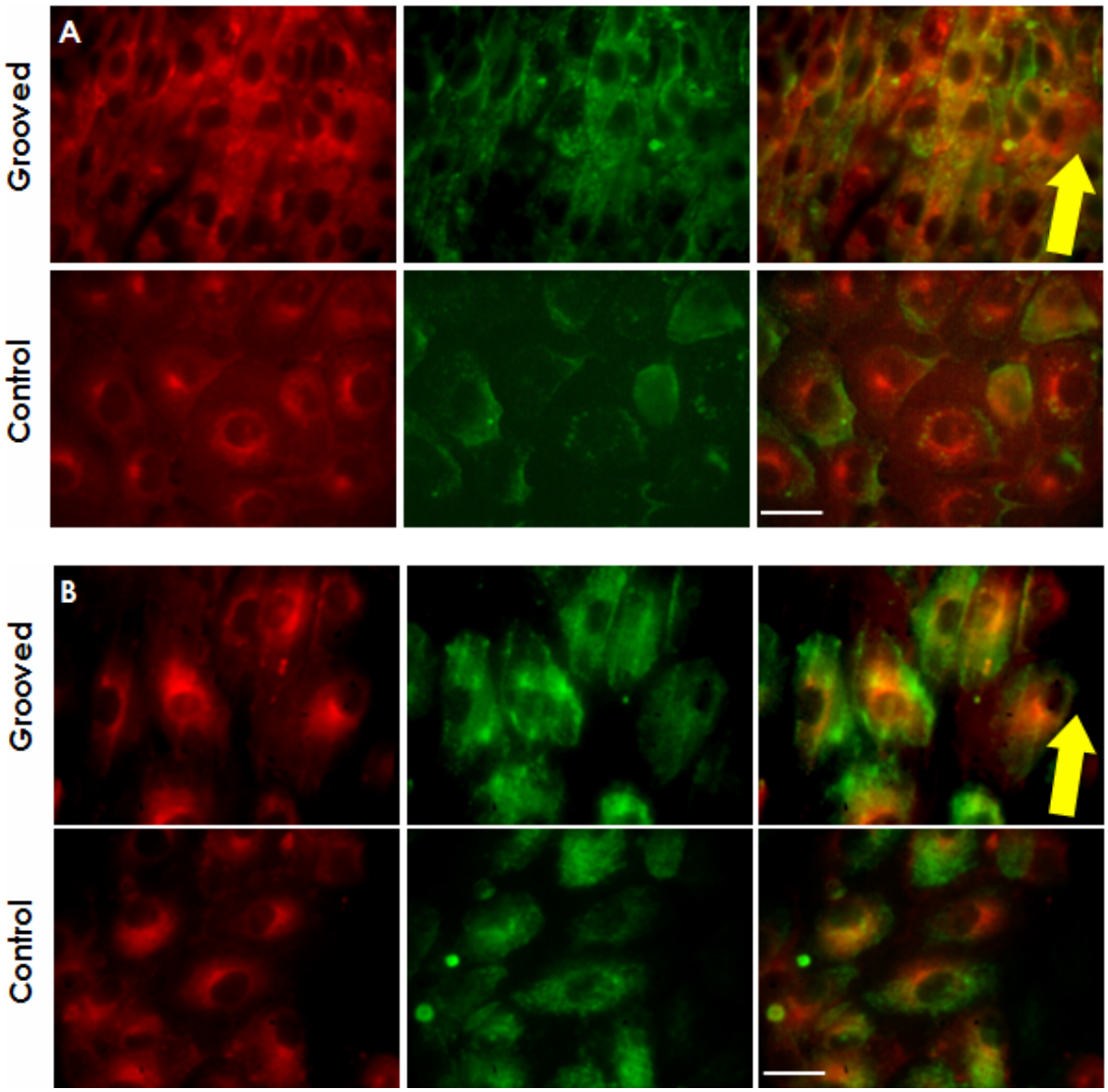


***Figure 12:*** *Fluorescent microscopy images of BAECs on both, grooved and smooth surfaces, for channel depths of 1 µm (A) and 5 µm (B). eNOS (red), Cav-1 (green) and merged channels show protein distribution. The 1 µm pattern shows a confluent monolayer of aligned cells with respect to the groove direction, along with increased levels of protein expression and high levels of protein colocalization (yellow pixels in the merged channel image). The 5 µm shows a decreased alignment in comparison to the 1 µm. The scale bar is 25 µm.*

Along with significant protein expression level differences, the 1 µm pattern shows high levels of protein colocalization (from the merged channel) compared to the smooth substrate, which is not observed for the other patterns. Comparatively, the 5 µm pattern shows a decrease in cell alignment relative to the groove direction (Figure 12B). On this pattern, protein expression levels are comparable between control and pattern substrates, and minimal colocalization may be depicted. A very important and interesting result of the BAECs on the 5 µm groove depth is that the channels are fluorescently labeled by eNOS and Cav-1 proteins, which signifies the fact that these proteins align along and within the channels and may be involved in the signaling mechanism that allows these cells to 'sense' variations in the surrounding microenvironment.

Some important observations have resulted from the nanoscale and microscale groove experiments. With increasing groove depth from 200 nm to 1 µm, cell alignment with respect to groove direction increased. However, a further increase in groove depth to 5 µm showed a decrease in cell alignment. These cell alignment studies showed differences in cell morphology between aligned and control cells. The BAECs that were aligned on grooved PDMS patterns depicted an elongated, stretched out morphology that would most accurately be approximated as an ellipse, while ECs on the smooth substrates depicted random, polygonal shapes that would accurately be approximated as a circle. These differences in cell shape between patterned and smooth samples are a combination of two factors, one being the cell orientation due to the underlying substrata, and the second is the cell elongation due to the parallel channels and ridges. Visually, the 1 µm substrate showed the most alignment of a confluent monolayer of endothelial cells along

with a significant increase in the protein expression levels on the groove patterns. This protein expression enhancement may be an artifact of the high level of cell alignment observed using these groove depth substrates. Also, the eNOS and Cav-1 distribution was punctate across the cell surface and at the borders of the cells on patterned surfaces as compared to eNOS being localized primarily within intra-cellular compartments, and Cav-1 dispersed across the cell surface on the non-patterned surfaces. Furthermore, the 5 µm pattern was the only groove depth to cause an alignment of proteins within the channels, which may be indicative of a signaling mechanism and/or a possible role of the cell cytoskeleton (e.g. actin filaments) in cell orientation. The orientation, elongation and morphology of endothelial cells on patterns and smooth surfaces will be quantified in the next couple sections.

#### 4.1.2.1 Cell orientation

Cell orientation was determined based on the angle of the cells with respect to the groove direction. Given the observation that aligned and control cells depicted elliptical and polygonal shapes respectively, an ellipse was used to approximate aligned cells while a circle was used for control cells. Cell direction was related to the longest axis that fit within the ellipse and circle approximations. On measuring the angle between the longest axis and the reference groove direction, the alignment or orientation of the cell was obtained. These measurements were performed using the Cav-1 channel (green) fluorescent images of PDMS patterns and controls because these staining images more clearly highlighted the cell boundaries, which made it simpler to outline cells for analysis

using the CellProfiler and ImageJ softwares. Also, it is important to note that the cell orientation for smooth substrates was determined based on an arbitrarily defined axis.

Cell orientation was recorded on a ±90º scale, where the positive and negative angles were considered positive for simplicity of plotting the results in a positive x- and y-axis graph. In order to compare the differences in cell orientation between patterned and control substrates, the histograms shown in Figure 13 (below) were created. The x-axis represents the angle between the cell's longest axis and the groove direction, which is the cell orientation (degrees), in bins of 5º while the y-axis represents the percentage incidence (%). It can be seen that alignment of the confluent monolayers of BAECs increases as the groove depth is increased from 200 nm to 1 µm, with a peak in the 500 nm – 1 µm range. A further increase in groove depth to 5 µm results in a decrease in cell alignment. These observations are consistent with the results of the visual analysis of the immunostaining images taken with a fluorescent microscope. The poor alignment of cells on the 200 nm pattern may be interpreted from the histogram (Figure 13) as consisting of two separate populations of cells, the major group exhibits cells with orientations in the 0-60º range, while the minor group exhibits cells with orientations in the 75-85º. The 500 nm and 1 µm histograms are similar in terms of the shape of the distribution, with the 1 µm showing an approximate normal distribution that is shifted along the positive x-axis. Another important observation from the histograms is the fact that the control substrates represent random cell orientation but minor differences exist in their distributions, which theoretically would be assumed to be identical across different PDMS substrates. The latter shows the importance of comparing patterns to their respective control surfaces.

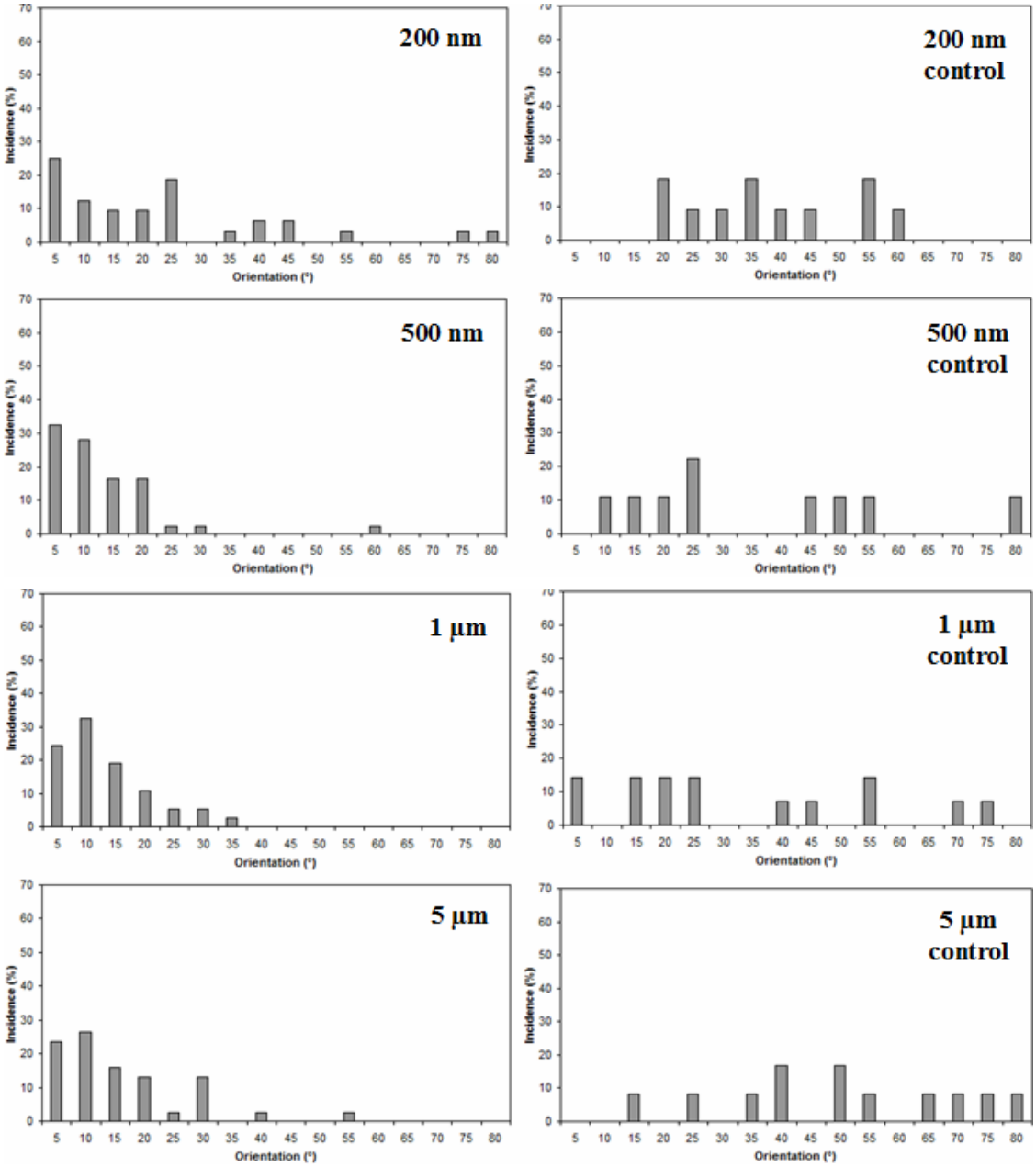


***Figure 13:*** *Histograms of BAECs cultured on grooved and smooth PDMS substrates for 24 h that helps visualize differences in cell orientations across the range of groove depths (200 nm - 5 µm) as well as between pattern and smooth (control) surfaces. The x-axis represents the cell orientation (degrees) and the y-axis represents incidence (percentage). The x-axis has been divided into 5º bins after comparing a range of bin sizes (2-10º) for the most useful data representation.*

Although the histogram representations of cell orientation distributions of BAECs on different groove depths were useful in showing differences between experimental groups, it is important to determine statistical significance of the results. To compare the population distribution of cell orientation between grooved patterns and smooth substrates, the Kolmogorov-Smirnov test (K-S test) of statistical significance was performed. The D-statistic of the K-S test represents the maximum difference between cumulative distributions, which once calculated was used to compute the probability value (*p*-value).

***Table 2:*** *Results of the Kolmogorov-Smirnov test of statistical significance to compare population distributions of cell orientation.*

| | **D statistic** | ***P*-value** |
|---|---|---|
| **200 nm** | 0.389 | 0.126 |
| **500 nm** | 0.492 | 0.010 |
| **1 µm** | 0.436 | 0.029 |
| **5 µm** | 0.417 | 0.060 |

At the 5% level of significance, it is observed that the 500 nm and the 1 µm groove depths resulted in statistically different cell orientation distributions as compared to their respective controls. This result validates the previously mentioned hypothesis that the critical groove depth that induces uniform alignment in a confluent monolayer of BAECs lies in the range of 500 nm – 1 µm. Further experimentation need to be conducted around

this range of channel depths to determine if improvements in alignment could be achieved relative to the results of the present study.

To compare the orientation between grooved patterns of different depths, cells were considered aligned if the angle between the longest axis and the groove direction was within ±15º (Yim et al., 2005). On the other hand, cells that exhibited an angle of 15-90º between their major axis and the grooves were considered non-aligned. Figure 14 shows a histogram of the percentage of aligned cells on grooved substrates after 24 h of incubation. Cell alignment increased from about 50% for the 200 nm patterns to about 80% for the 500 nm and the 1 µm patterns respectively and slightly decreased to about 65% for the 5 µm pattern.

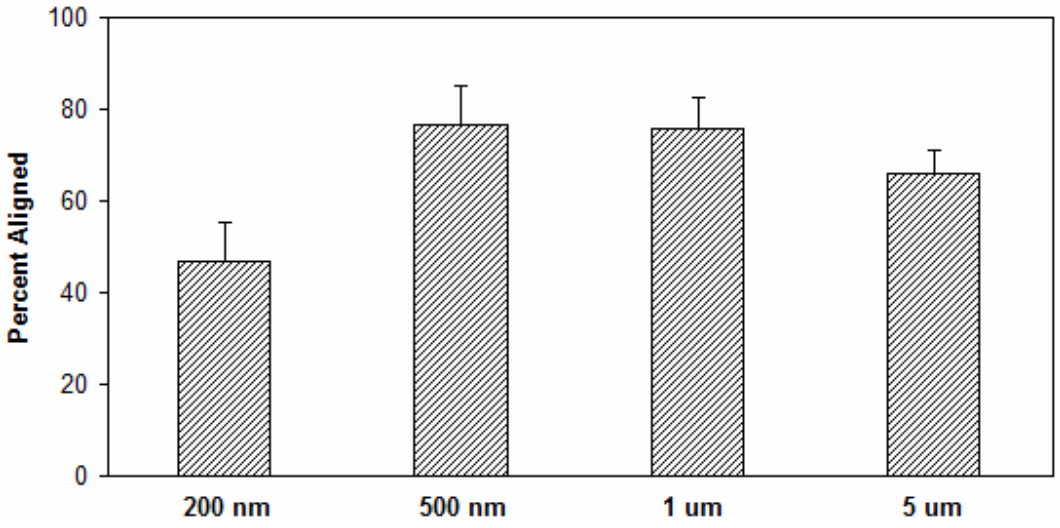


***Figure 14:*** *Histogram showing the percentage of BAECs aligned on grooved substrates with depths of 200 nm – 1 µm. Data represents mean ± standard deviation (SD).*

In this study of cell orientation, a comparison of the 200 nm, 500 nm, and 1 µm patterns shows that small increases in the groove depth (e.g. few hundred nanometers) significantly enhances the cell response to align in the direction of the grooves, especially considering that these patterns have identical channel and ridge widths. It is inferred through this study that cell alignment depends heavily on the dimension of groove depth, where the 500 nm - 1 µm range was found to be critical in order to create a uniformly aligned confluent layer of endothelial cells. The next parameter to quantify cell shape is the elongation index, which gives insight regarding the morphology of cells as well as the spreading of cells on the grooved PDMS substrates.

#### 4.1.2.2 Cell elongation

The elongation index (Factor E) was calculated using the major and minor axes of the ellipse approximations of BAECs to compare cell shape on patterned and smooth substrates (Yim et al., 2005). This parameter describes the extent the cell is lengthened of stretched out, which is a cell response to variations in the underlying microtopography (Andersson et al., 2003). From the histogram (Figure 15), it is observed that cells on the smooth (control) surfaces exhibit the smallest value of Factor E (~0.8±0.3), which indicates that these cells are more accurately approximated as circular in shape rather than elliptical. With respect to the groove patterns, increasing the groove depth from 200 nm to 1 µm resulted in a gradual increase in the Factor E value from about 2.0 to 4.0, while a further increase in groove depth to 5 µm showed a decrease in the Factor E value to ~1.8. The maximum elongation index or Factor E value (~4.0) is found on the 1 µm

PDMS groove substrates, which makes this groove depth critical in inducing cell alignment as well as cell elongation in confluent monolayers of BAECs.

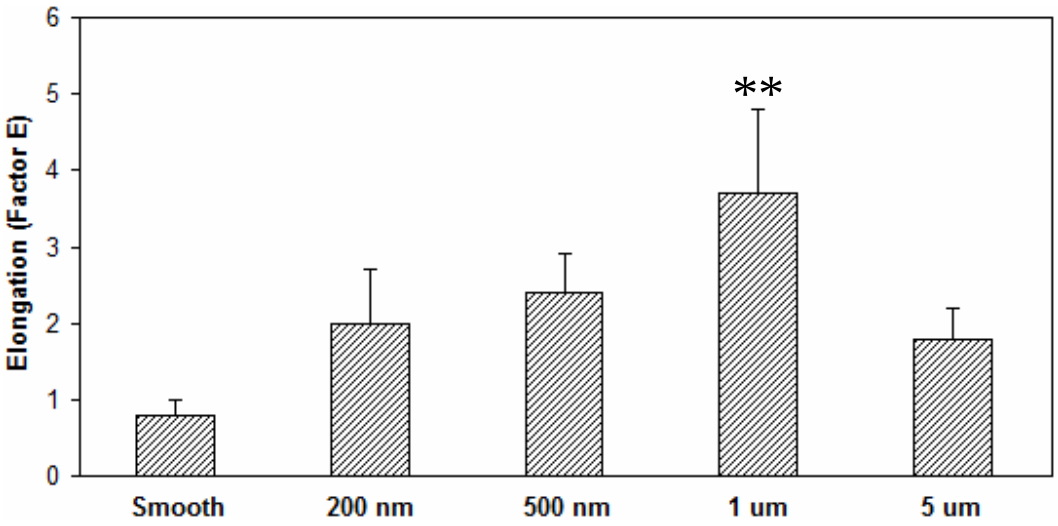


***Figure 15:*** *Histogram of BAEC elongation (based on Factor E) showing the fact that cells on groove patterns exhibit greater elongation indices as compared to the smooth surfaces. Among the different groove depths, it is observed that the 1 µm pattern is critical in creating cells that are highly elongated (Factor E ~4.0). Data represents mean ± standard deviation (SD) for 30-40 cells per experimental group.*

The above results were assessed for statistical significance by performing a Student's t-test. The test results demonstrated that the 1 µm pattern elongation index is significantly greater than the smooth substrate, and the other patterned substrates (200 nm, 500 nm, 5 µm) at the 1% level of significance ($p < 0.01$). These observations show that cell

elongation varies with groove depth and is maximized on the 1 µm substrates for a culture time of 24 h.

#### 4.1.2.3 Cell morphology

From the fluorescent microscopy images of confluent BAECs on grooved PDMS substrates shown in Figures 11A, 11B, 12A, 12B, cell morphology on smooth, 200 nm, 500 nm, 1 µm, and 5 µm surfaces may be examined. Consistently, cells on smooth surfaces display a polygonal or circular shape with random orientations, while cells on the grooved substrates display an elliptical shape with their longest axes aligned along the groove direction.

On smooth substrates (Figure 11A), a majority of the cells appear polygonal, while a small number of cells display elongated structures in any random direction. Comparatively, BAECs on the grooved patterns with channel depths of 200 nm – 5 µm display a majority of cells aligning in the direction of the grooves with an elliptical or stretched out morphology due to their interaction with the underlying microtopography. On the 200 nm and 5 µm PDMS (Figures 11A, 12B), elongated cells exhibit major axes either parallel to the channels or across several ridges and channels. For the 200 nm, the cells do not show specific responses to the 200 nm groove depth as seen for the 5 µm substrates, where the cells express proteins that may be involved in the 'sensing' process by aligning within the channels. On the 500 nm and 1 µm patterns (Figures 11B, 12A), the majority of the cells display long axes that are parallel to the channels and a small

number of cells that elongate across multiple ridge/channel boundaries. Based on the previously discussed cell orientation and cell elongation parameters, these cell morphology observations remain consistent, further validating the 1 µm groove depth as the most optimized for alignment.

### 4.2 Two-dimensional patterns of protein can regulate cell orientation

The two-dimensional and three-dimensional shape of cells in vivo play different roles in regulating functions of these cells. Although PDMS substrates with nano- and micro-grooves allows for the study of endothelial cells in a static environment, a major limitation of this method is that the results consider cell orientation and protein localization due to groove width and periodicity (2D), and groove depth (3D), as one factor. An experimental technique is required that may allow for the identification of the role of 2D and 3D cues in cell orientation, independent of each other. To address this need, microcontact printing techniques must be developed that mimicked the alternating, parallel channels and ridges of the PDMS microgroove substrates by printing the ECM protein, fibronectin, in parallel patterns. The use of microcontact printed patterns (as described in section 3.3) provides a method to study cell shape under static conditions with respect to 2D cues alone, which have been shown to affect intracellular structures including cytoskeletons, microtubules, actin fiber formation, signaling pathways, and cellular functions (Vartanian et al., 2008).

Despite many reports on the effects of substrate topography on cells, the independent effect of 3D parameters on cell alignment has not been investigated (Choi et al., 2007). The primary expectation of this research is to develop a method to print micropatterns of fibronectin, the extracellular matrix protein, mimicking the parallel grooves structure of the PDMS substrates utilized for the Cav-1 and eNOS staining experiments in the previous sections. This will help identify the independent role of 2D cues in microtopography-induced cell alignment changes. In addition, these fibronectin micropatterns will be employed to quantify cell alignment in the direction of grooves, in this case, grooves of fibronectin. To remain consistent with the microgroove experiments, the protein patterns will be made on smooth poly(dimethylsiloxane) (PDMS) substrates. The protein pattern width was varied in the micro-scale, specifically 10–200 µm, to account for the different mechanical cues that may be involved in shaping of cells. Since these 2D patterns were of fibronectin monolayers, the height dimension was insignificant as confirmed by published reports (Vartanian et al., 2008). Therefore, any differences in cell alignment and protein localization were attributed to the variation in the pattern width. Similar to the PDMS microgroove experiments, these patterns were cultured with BAECs and stained for important signaling proteins, Cav-1 and eNOS, to investigate cell orientation and cell morphology. Further, these patterns were used to study the cellular distribution of Cav-1 and eNOS as well as the percentage colocalization, which are discussed in later sections.

The results showed that the 200 µm wide FN pattern had two populations of cells, one group that were primarily circular in shape, and the other group that had their long axes

parallel to the boundary of the FN pattern. Aligned cells did not display enhanced levels of protein expression, which was much lower on these FN patterns as compared to the BAECs on PDMS microgrooves. When the FN pattern width was decreased to 10 µm, the cells were about 100% aligned, which confirms that cell orientation is a result of 2D surface geometry and 3D spatial arrangement. In addition to cell morphology, cell orientation analyses were performed using the BAECs on these FN patterns.

### 4.2.1 Microcontact printed substrate characterization

The printing of fibronectin was carried out using smooth PDMS surfaces and elastomeric stamps fabricated using silicon wafers with 200 µm wide channels, which were obtained from the Vascular Kinetics Laboratory. These elastomeric stamps were used to print 200 µm wide patterns of fibronectin on smooth surfaces, at a protein concentration of 10 µg/mL, in order to remain consistent with the PDMS microgroove experiments. Similarly, 10 µm wide patterns of FN were printed for experimentation with BAECs.

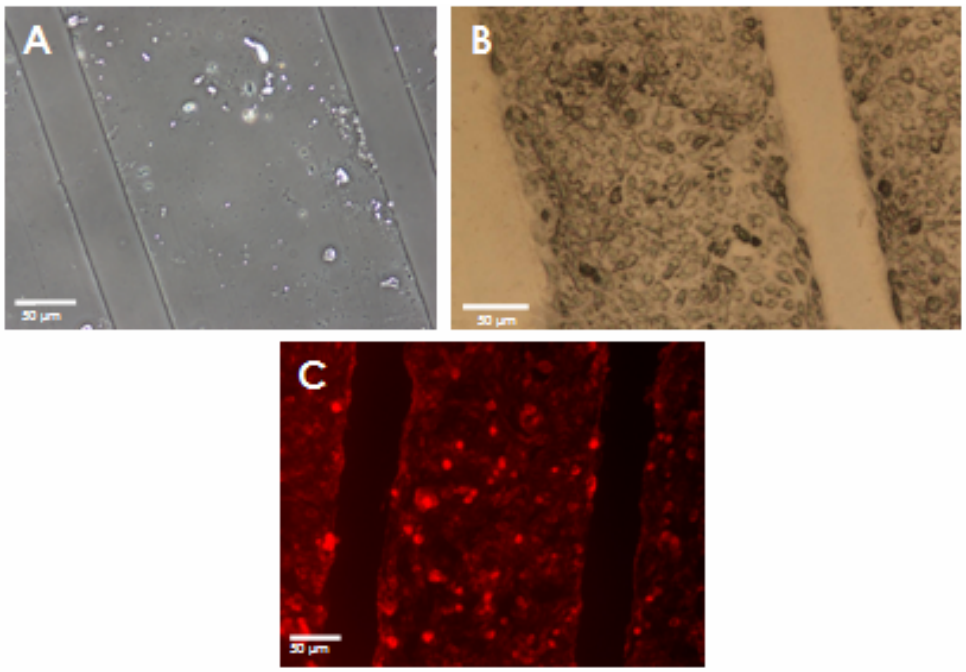


***Figure 16:*** *200 µm wide patterns of fibronectin after the printing process (A; light microscope), patterns incubated with BAECs (B; light microscope), and BAECs fluorescently labeled with antibodies against eNOS (C; fluorescent microscope).*

Ideally, the characterization of the fibronectin printed PDMS should be carried out using an antibody that recognizes the protein of interest (in this case, fibronectin). However, since such antibodies are extremely expensive, this method was not economical viable for this project's scope. To confirm successful microcontact printing of fibronectin patterns, first, the smooth PDMS substrates were rinsed with phosphate buffered saline and imaged under a light microscope (Figure 16A), which confirmed the presence of 200 µm wide patterns. However, this does not demonstrate that fibronectin is specifically printed within the parallel lines observed under a light microscope. Secondly, the printed patterns

were cultured with BAECs for 8 h and imaged using a light microscope, which showed the presence of confluent layers of cells within the protein printed boundaries (Figure 16B). This second test result supports the fact that fibronectin was specifically printed using the microcontact printing technique discussed in section 3.3. Further, the BAECs cultured on these patterns of FN were fluorescently labeled with antibodies that recognized eNOS, which clearly helped visualize 200 µm wide patterns of cells (Figure 16C). The results so far confirm successful printing of FN by the presence of cells only within 200 µm wide patterns and without any cells in the 10-20 µm gaps between protein boundaries (Hannachi et al., 2009).

Based on these results, it is clear that the microcontact printing resulted in uniform patterns of fibronectin, which allows differences in cell orientation and protein localization between randomly oriented and aligned cells to be attributed to variations in the location of the cells (in this case, the mid section of the pattern versus the pattern boundary).

### 4.2.2 Endothelial cell shape: 2D surface geometry and/or 3D spatial arrangement

In this study, BAECs cultured on 10-200 µm wide fibronectin patterns printed on smooth PDMS surfaces were quantified with respect to cell orientation relative to the protein pattern boundary. Similar to the PDMS microgroove quantification, this parameter was selected since it has been the most commonly used method to describe cell shape in published studies. This allows for a discussion to determine whether any relationships

between cell shape and underlying two-dimensional protein patterns observed in this study is comparable to the previously discussed microgroove experiments (2D and 3D cues). In addition to orientation, cell morphology was compared between BAECs in the mid section of the 200 µm wide patterns and those at the edge of the protein patterns.

Once again, to visualize BAECs on 2D fibronectin patterns, the cells were fluorescently labeled using antibodies that recognized two regulatory signaling proteins, Cav-1 (green channel) and eNOS (red channel) (Figure 17). The smooth PDMS surfaces required for printing were prepared by film casting PDMS on the surface of non-patterned silicon wafers. Since the printed substrates exhibited both orientations of BAECs, specifically, the randomly oriented and circular cell shape as well as the elongated, aligned and elliptical cell shape, the mid section of the pattern was compared to the end section (edge) of the same pattern. For the purposes of this study, the mid section was considered the control region while the end section was the aligned region. All experiments compared control and aligned regions of the same FN printed substrate to take into consideration any minor differences in protein coverage of the specific PDMS surface.

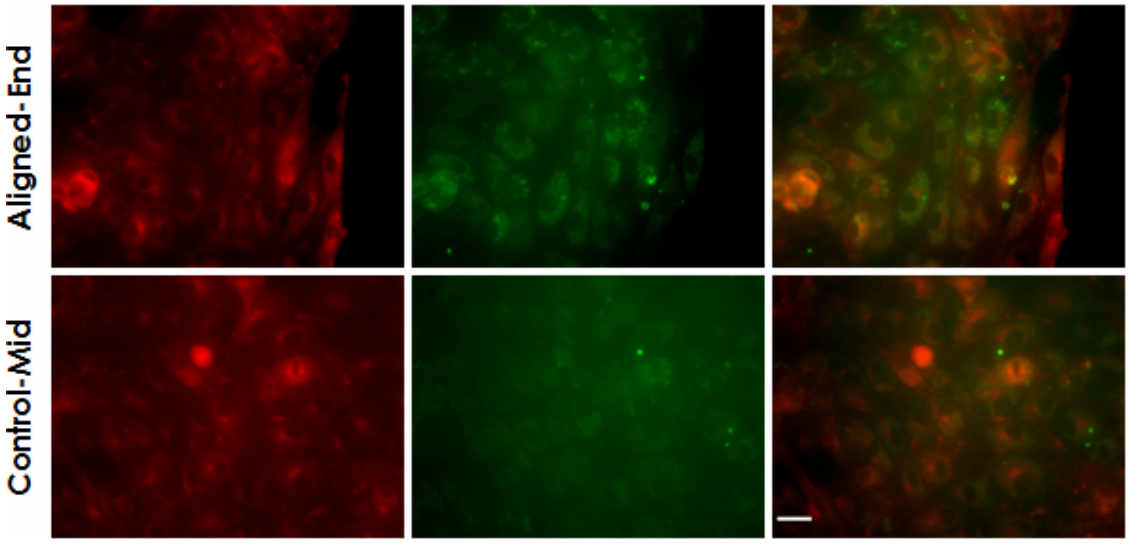


***Figure 17:*** *Fluorescent microscopy images of BAECs on 200 µm fibronectin patterns showing randomly oriented (circular) cells in the mid section of the pattern and elongated, aligned (elliptical) cells in the edge region of the pattern. For this study, the mid section was considered the control sample, while the edge region was the aligned sample. eNOS (red), Cav-1 (green) and merged channels show protein distribution. The scale bar is 25 µm.*

Figure 17 (above) shows the effects of two-dimensional fibronectin patterns (200 µm) on BAEC orientation and elongation. The aligned section images show the fibronectin boundary, which is used as the reference direction to quantify cell orientation. It is observed that two populations of cells exist on within the fibronectin patterns, some cells that tend to orient parallel to the direction of the boundary (end section), while others exhibit random orientations that are similar to cells on smooth surfaces (mid section). The effect of the 2D boundary of fibronectin in aligning BAECs without a 3D parameter is demonstrated in the end section of the pattern. In terms of protein expression levels, the

aligned cells near the FN boundary do not show significant differences compared to their counterparts (non-aligned cells) in the middle section of the pattern. The latter represents the fact that alignment of cells due to the FN boundary did not enhance levels of eNOS and Cav-1 expression. In addition, no significant colocalization differences were observed (visually), and neither was there differences in the cellular distribution of proteins between aligned and control cells. In terms of morphology, the aligned cells show approximate elliptical shape while the control shows a combination of circular and elliptical shaped cells, with a majority of circular shaped cells.

After making some observations about 200 µm wide patterns of fibronectin and their effects on cell orientation, it is important to consider 10 µm wide FN patterns as shown in Figure 18. Specifically, the figure shows BAECs cultured on 10 µm wide patterns of fibronectin that were subsequently visualized using immunostaining. It is important to note that this pattern does not represent a confluent monolayer of BAECs, but this experiment was performed to determine whether cell orientation changes are a result of 2D surface geometry, 3D spatial arrangement of cells, or a combination of the two. These results were not compared to the PDMS microgroove data. However, the 200 µm wide FN patterns depicted confluent monolayers of BAECs and were compared to the PDMS microgroove experiments to observe differences in cell orientation and protein colocalization. The 10 µm wide FN pattern shows about 100% cell alignment in the direction of the protein boundaries, along with higher levels of protein expression and protein colocalization (yellow pixels in the merged channel) compared to the 200 µm wide FN pattern.

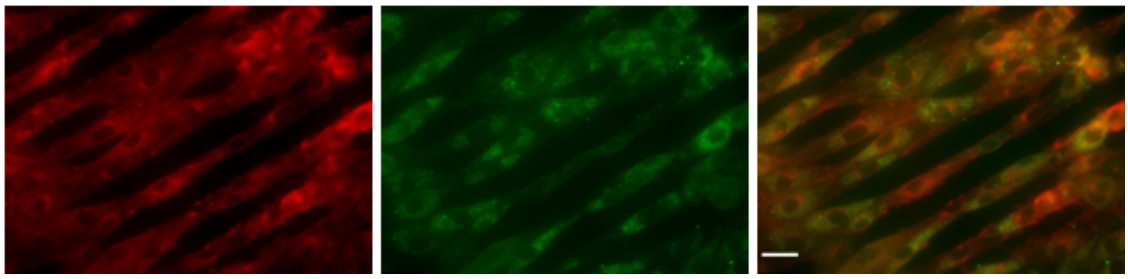

***Figure 18:*** *Fluorescent microscopy images of BAECs on 10 µm wide fibronectin patterns printed on smooth PDMS surfaces. eNOS (red), Cav-1 (green) and merged channels show protein distribution. These images do not represent a confluent monolayer of BAECs. However, it is clear that about 100% cell alignment exists with respect to the protein boundaries, along with high levels of protein expression and protein colocalization (yellow pixels in the merged channel image). The scale bar is 25 µm.*

A very important and interesting result of the BAECs on the 10 µm wide FN patterns is that the high levels of cell alignment parallel to the protein boundary direction demonstrates the dependence of cell orientation on the width of the underlying 2D protein pattern. Based on these observations, it is confirmed that cell orientation is a result of two factors, one being cues from the 2D surface geometry, and the other being cues from the 3D spatial arrangement of cells. Further, it is seen that these microcontact printed patterns allow for the investigation of cell shape due to 2D geometry that is independent of 3D cues. Using a combination of PDMS microgrooves and microcontact printed protein patterns it is possible to compare cell orientation mechanisms due to 2D and 3D factors independently of each other. The orientation and morphology of endothelial cells on fibronectin patterns (including the end and mid sections) will be quantified in the next couple sections.

#### 4.2.2.1 Cell orientation and morphology

Similar to the PDMS microgroove analysis, cell orientation was determined based on the angle of the cells with respect to the groove direction. Cell direction was related to the longest axis that fit within the ellipse (aligned cells) and circle (control cells) approximations. On measuring the angle between the longest axis and the reference protein boundary, the alignment or orientation of the cell was obtained. These measurements were performed using the Cav-1 channel (green) fluorescent images of BAECs on the 200 µm wide fibronectin patterns. Different from the PDMS microgroove analysis, cell orientation for control cells (mid section) was determined based on the same reference protein boundary used for the aligned cells.

In order to compare the differences in cell orientation between aligned and control sections of the printed FN patterns, the histograms shown in Figure 19 (below) were created. It can be seen that alignment of the confluent monolayer of BAECs increases as distance between the cells and the protein boundary decrease. These observations are consistent with the results of the visual analysis of the immunostaining images taken with a fluorescent microscope. The increase in alignment of cells in the end section of the 200 µm wide FN pattern may be interpreted from the histogram as consisting of two separate populations of cells, the major group exhibits cells with orientations in the 0-30º range, while the minor group exhibits cells with orientations in the 40-85º range. Comparing this result with the histogram of the mid section of the FN pattern, it is seen that there was a shift in randomly oriented cells with orientations in the range of 30-85º to the two

populations of cells seen in the end section histogram. The end section and mid section histograms are different in terms of the shape of the distributions, with the end section showing an approximate bimodal distribution and the mid section showing a right-skewed distribution.

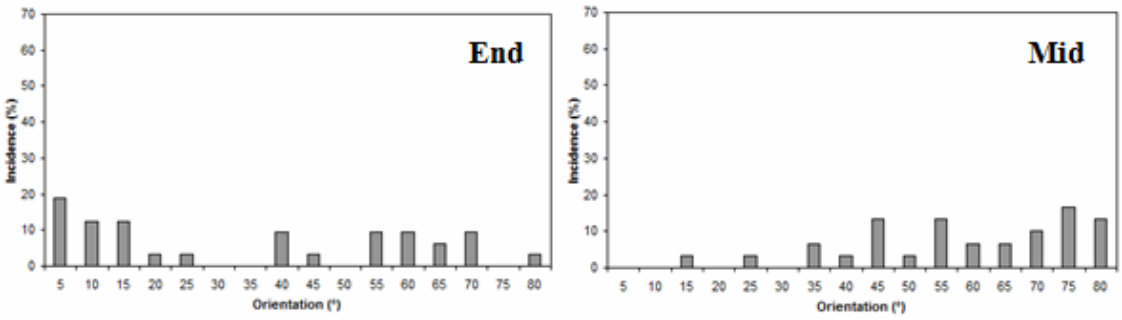


***Figure 19:*** *Histograms of BAEC orientation cultured on 200 µm wide patterns of fibronectin for 24 h, showing the mid and end sections of the protein pattern that helps visualize differences in cell orientations as the protein boundary is approached. The x-axis represents the cell orientation (degrees) and the y-axis represents incidence (percentage). The x-axis has been divided into 5º bins after comparing a range of bin sizes (2-10º) for the most useful data representation.*

The histogram representations of cell orientation distributions of BAECs on aligned and control sections of the 200 µm wide FN pattern were useful in showing differences between experimental groups, but it is important to determine statistical significance of the results (as done for the PDMS microgroove experiments). The population distribution of cell orientation between aligned and control sections were compared by computing the

Kolmogorov-Smirnov test (K-S test) of statistical significance. The D-statistic of the K-S test was calculated and used to calculate the probability value (*p*-value). The K-S test resulted in a D-statistic value of 0.4187 with a corresponding *p*-value of 0.006. This value demonstrates that the aligned section of the 200 µm FN pattern is significantly different compared to the control section of the pattern at the 1% level of significance ($p < 0.01$). From the latter, it is clear that the FN boundary acts like a grooved pattern in that it causes the BAECs to align parallel to the edges of the printed pattern.

Furthermore, the orientation between aligned and control sections of the FN pattern was compared by considering cells as aligned if the angle between the longest axis and the FN boundary was within ±15º (Yim et al., 2005). Cells that exhibited an angle of 15-90º between their major axis and the FN boundary were considered non-aligned. Based on this definition, it is observed that the alignment of cells (mean ± SD) increased from 3.33 ± 1.92% to 43.75 ± 3.61% for the control section to the aligned section of the 200 µm wide FN pattern. To confirm statistical significance, a Student's t-test was performed on these orientation values and resulted in a *p*-value of 0.005, which is significant at the 1% level of significance. These results demonstrate the drastic effect the FN boundary had on the confluent monolayer of BAECs that were randomly oriented and on contact with the boundary shifted to a more aligned orientation.

In this study of cell orientation, a comparison of the mid section to the end section of a 200 µm FN pattern shows that a 2D protein boundary may significantly enhance the cell responses to align in the direction of the boundary, for up to 80 µm away from the pattern

edge. It is inferred through this study that cell alignment depends heavily on the 2D surface geometry of the underlying substrate and therefore, on the PDMS microgroove surfaces, the BAECs were responding to 2D cues due to the surface and 3D cues due to the spatial arrangement of cells within channels. The latter is confirmed by quantifying the alignment of BAECs on the 10 µm wide FN patterns, which as expected, resulted in 100% alignment. This result validates the observation that cell orientation is dependant on the 2D surface geometry.

Another parameter that must be considered to get an understanding of the effects of 2D surface geometry on BAECs is cell morphology. From the fluorescent microscope images of confluent BAECs on 200 µm FN patterns shown in Figure 17, cell morphology in aligned (end) and control (mid) sections may be examined. Consistently, cells on control sections display a polygonal or circular shape with random orientations, while cells near the FN boundary display an elliptical shape with their longest axes aligned along the boundary direction. On control sections, a majority of the cells appear polygonal, while a small number of cells display elongated structures in any random direction. In addition, the control sections show a large number of cells that are approximately perpendicular in orientation to the fibronectin boundary. Comparatively, BAECs on the aligned sections display a majority of cells aligning in the direction of the protein boundary with an elliptical or stretched out morphology. Based on the previously discussed cell orientation parameter, these cell morphology observations are accurate.

### 4.3 Cellular distribution of eNOS and Cav-1 on microgrooves and FN patterns

To observe differences in the spatial localization of Cav-1 and eNOS on microgrooves as compared to smooth substrates, as well as differences on microcontact printed patterns, 3D surface plots were developed. The plot display color scheme was selected as the fire LUT since it enhanced small differences between experimental and control images. In this study, the individual cells were cropped from 2D fluorescent images (following background subtraction) and visualized in 3D.

Figure 20 (below) shows the cellular distribution of eNOS and Cav-1 for the 1 µm groove depth pattern and its respective control (smooth) substrate. This pattern was selected since it was accepted as the critical groove depth necessary to induce maximum cell alignment, cell elongation, protein expression, and protein colocalization of a confluent monolayer of BAECs. Therefore, distribution of proteins in BAECs cultured on this specific groove depth may provide insights into the expression levels of these proteins in vivo, which may help identify signaling mechanisms involved in cell shape changes. Based on the intensity scale bar, it is seen that the levels of eNOS and Cav-1 expression are several fold greater than their counterparts on the smooth substrates. In terms of protein localization, Cav-1 appears to be distributed along the cell periphery for the control substrates (Figure 20C), while they are located right next to the nucleus (juxtanuclear) in the aligned cells (Figure 20A). On the other hand, eNOS appears to be clustered in the form of aggregates in the cell cytoplasm for the control cells (Figure 20D), while they shift to a juxtanuclear position in the aligned cells (Figure 20B).

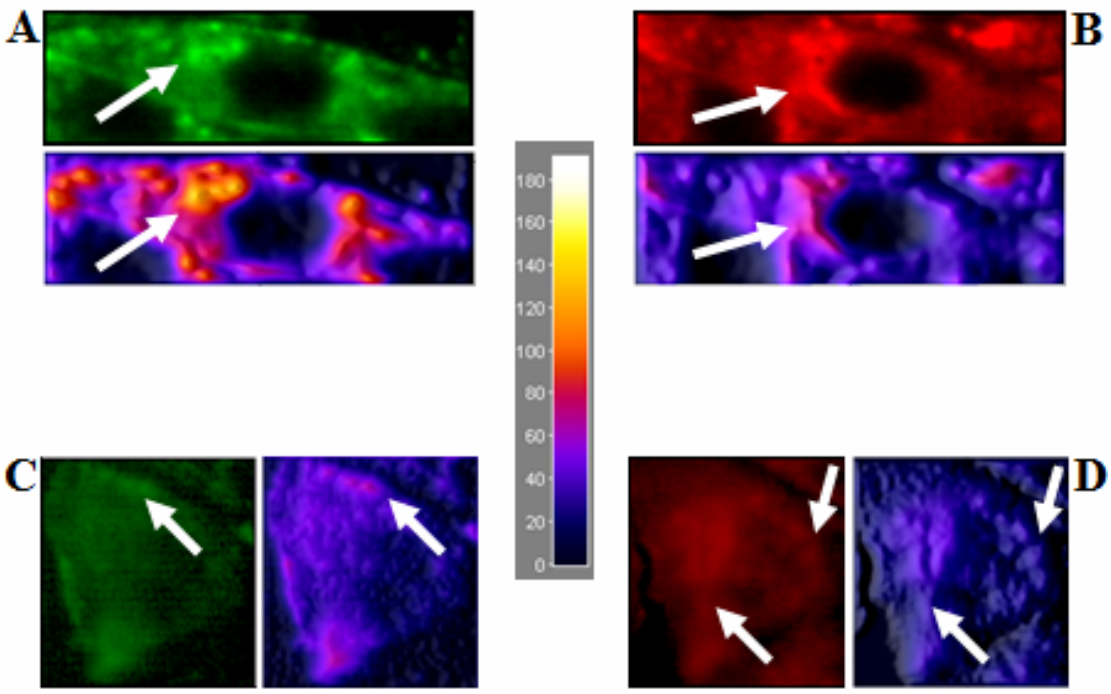


***Figure 20:*** *3D surface plots of BAECs cultured on the 1 µm groove depth pattern (A, B) and their respective controls (C, D). Cav-1 localization appears to be juxtanuclear for the aligned cells (A) and shifts to a peripheral distribution on the control cells (C). eNOS localization appears to be cytoplasmic for the control cells (D), which changes to juxtanuclear in the aligned cells (B). Protein expression levels are clearly enhanced on the patterned substrates (A, B) as compared to the smooth surfaces (C, D). The white arrows indicate protein localization, and the intensity bar is shown in the center.*

Similarly, Figure 21 displays the cellular distribution of eNOS and Cav-1 for the 200 µm fibronectin pattern, for the aligned and control sections of the pattern. This printed FN width was selected since it successfully induced alignment in the cells closer to the protein boundary, while maintaining randomly oriented cells in the middle section of the protein pattern. Therefore, comparing aligned versus control sections was simple and

accurate since minor variations in surface geometry are assumed constant within an individual PDMS substrate. Distribution of proteins in BAECs cultured on this specific protein width pattern may provide insights into the expression levels of these proteins in response to 2D cues independent of 3D factors. This may allow for a better understanding of the differences between 2D and 3D cues in terms of cell orientation, protein expression, and protein colocalization changes. Based on the intensity scale bar, it is seen that the levels of eNOS and Cav-1 expression are similar for aligned cells and their control counterparts. In terms of protein localization, Cav-1 appears to be distributed in the cytoplasm for both circular (Figure 21C) and elliptical cells (Figure 21A), while eNOS remains juxtanuclear for both, aligned (Figure 21B) and control (Figure 21D) cells.

This study resulted in some very critical observations about the effects of underlying microtopography on the expression and distribution of proteins. Starting with the 200 µm FN pattern, it was observed that the protein expression levels of eNOS and Cav-1 between aligned and control cells were unchanged. Additionally, the spatial localization of these proteins remained constant across the circular and elliptical shapes, specifically, juxtanuclear distributions of eNOS and cytoplasmic distributions of Cav-1. Comparatively, the 1 µm groove depth PDMS pattern and its respective control surfaces showed significantly different results. The expression levels of eNOS and Cav-1 were several fold enhanced in the aligned cells as compared to the control cells, based on the intensity scale bar. Further, the distributions of eNOS and Cav-1 changes from cytoplasmic to juxtanuclear and peripheral to juxtanuclear respectively, for a shift from

control to aligned cells. These results demonstrate that the changes in protein expression levels and distribution are primarily regulated by the 3D spatial arrangement of cells.

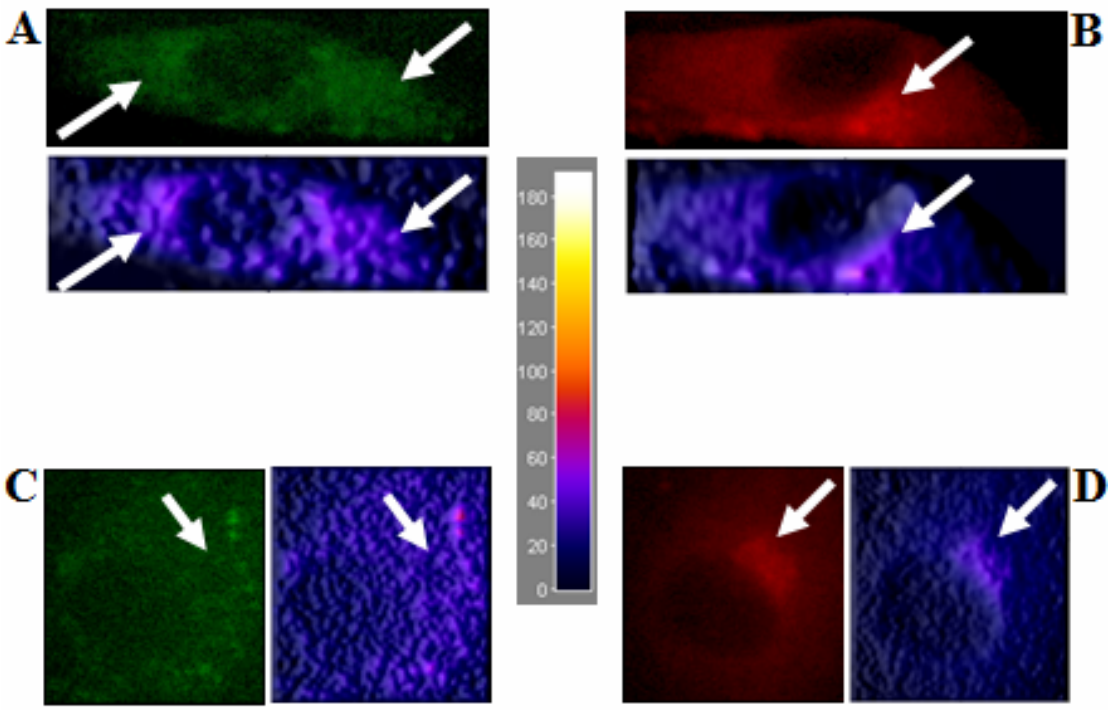


***Figure 21:*** *3D surface plots of BAECs cultured on the 200 µm fibronectin pattern including aligned (A, B) and control (C, D) sections of the pattern. Cav-1 localization appears to be cytoplasmic for the aligned (A) and control (C) cells. eNOS localization appears to be juxtanuclear for the control (D) and aligned (B) cells. Protein expression levels are unchanged on the aligned sections (A, B) as compared to the smooth sections (C, D). The white arrows indicate protein localization, and the intensity bar is shown in the center.*

### 4.4 Colocalization of signaling proteins: Cav-1 and eNOS

In addition to the cellular distribution of proteins, many research groups have quantified protein colocalization in search for possible roles of interacting proteins in regulating certain cell functions. In this research study, the colocalization of eNOS and Cav-1 were quantified to compare values across the 200 nm – 5 µm groove depth range as well as the 200 µm wide FN patterns. The colocalization parameter used is known as the Mander's Coefficient (R) (Manders et al., 1993). This coefficient of colocalization was selected for the simplicity of interpretation of the coefficient on the 0 – 1 scale and it's compatibility with fluorescent microscopy experiments. Prior to quantifying colocalization of proteins using the fluorescent images, background subtraction was performed using the ImageJ software since all image quantification methods are extremely sensitive to noise. Along with the Mander's Coefficient of colocalization, results were validated by analyzing frequency and red-green scatter plots. Furthermore, intensity correlation quotient (ICQ) plots of both channels of the images, red and green, are compared to determine whether the red and green pixel intensities vary in a dependent or independent manner.

Figure 22 (below) shows the colocalization analysis performed for the 1 µm groove depth PDMS pattern. The red-green scatter plot (Figure 22A), the frequency scatter plot (Figure 22B), the ICQ plots for the red channel (Figure 22C) and the green channel (Figure 22D) are presented. For the scatter plots, the intensity of the red pixels is shown along the x-axis while the intensity of the green pixels is represented along the y-axis. The red-green scatter plot displays the actual red, green, and yellow (colocalized) pixels of the

fluorescent images that are above the threshold of the image, which can be easily related to the original images. Although it is observed that there are several yellow pixels in the red-green scatter plot, a frequency scatter plot makes it clear as to what percentage of all the pixels above threshold are the colocalized pixels. The frequency scatter plot is pseudocolored with the hot colors representing colocalized pixels, which can be seen in red and some light green. In addition, from comparing the ICQ plots it is determined that the red and green pixels vary synchronously (dependent), which indicates that the overlapped pixels are not an artifact of random association. The Mander's Coefficient for the 1 µm groove depth is 0.76, which represents a colocalization of 76%.

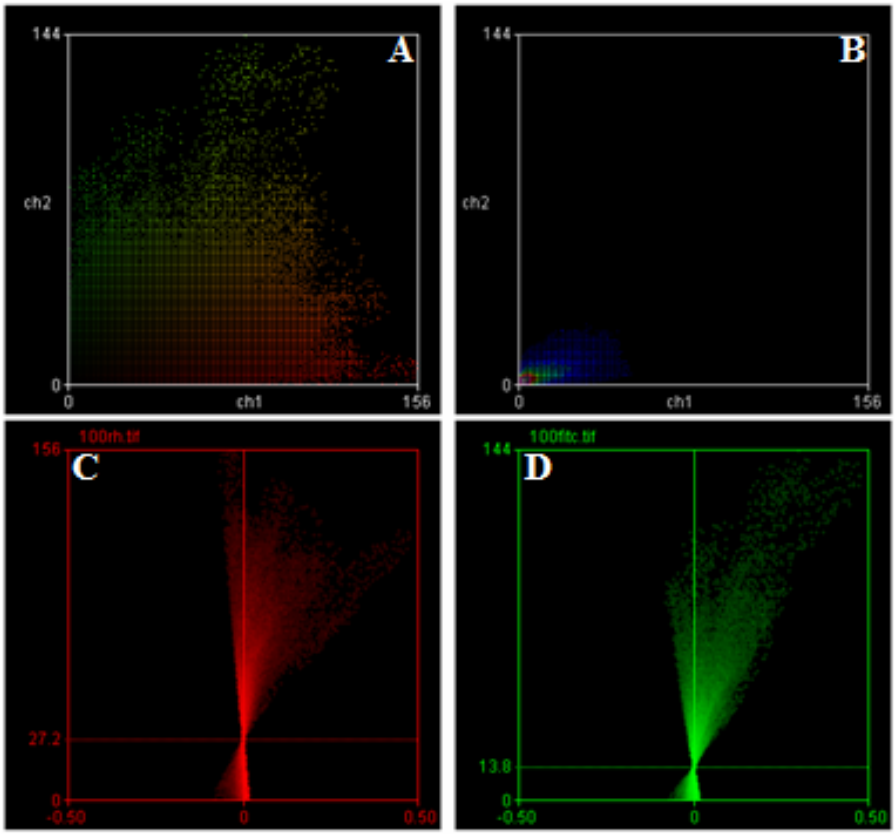


***Figure 22:*** *Colocalization analysis for the 1 µm groove depth PDMS pattern showing the red-green scatter plot (A), the frequency scatter plot (B), the ICQ plots for the red (C) and green (D) channels. The scatter plots represent the intensity of the red pixels along the x-axis and intensity of the green pixels along the y-axis. The ICQ plots represent the product of the differences from the mean (PDM) on the x-axes while pixel intensities are represented on the y-axes.*

To compare the 1 µm groove depth results, Figure 23 shows the colocalization analysis performed for the 1 µm control PDMS substrate. Once again, the red-green scatter plot (Figure 23A), the frequency scatter plot (Figure 23B), the ICQ plots for the red channel (Figure 23C) and the green channel (Figure 23D), are shown in the figure. It is observed

that there are few yellow pixels in the red-green scatter plot, which in terms of the frequency scatter plot is observed to display some red pixels. An important observation is that the ICQ plots show that the red and green pixels vary asynchronously (independent), which indicates that the overlapped pixels are an artifact of random association. Although a colocalization coefficient may be calculated for these plots, the actual colocalization is smaller in magnitude. The Mander's Coefficient for the 1 µm control substrate is 0.53, which represents a colocalization of 53%.

Based on the above analysis for the 1 µm groove depth and it's respective control surface, it is determined that there is high levels of colocalization on the 1 µm depth, while there is minimal colocalization on the smooth substrate, which is a result of random association. The latter are consistent with the observations made from comparing the colocalization plots of the 1 µm groove and control surfaces. Briefly, it may be observed that the red pixels in the frequency scatter plot for the 1 µm groove sample (Figure 22B) is significantly larger as compared to those for the 1 µm control sample (Figure 23B). In addition, the same is true by comparing the red-green scatter plots of the groove and control sample, where the number of yellow pixels is greater for the groove sample. Similarly, the above colocalization analysis was performed for the 200 nm, 500 nm, 5 µm, and 200 µm FN patterns. The results of these analyses are shown in the Figure 24, which displays a histogram of the percentage of colocalization for the different substrates. One consistent result for all the control samples of the microgroove experiments was that the ICQ plots showed independent variations between the red and

green pixel intensities, which represent the fact that these samples show colocalization that is primarily random in nature.

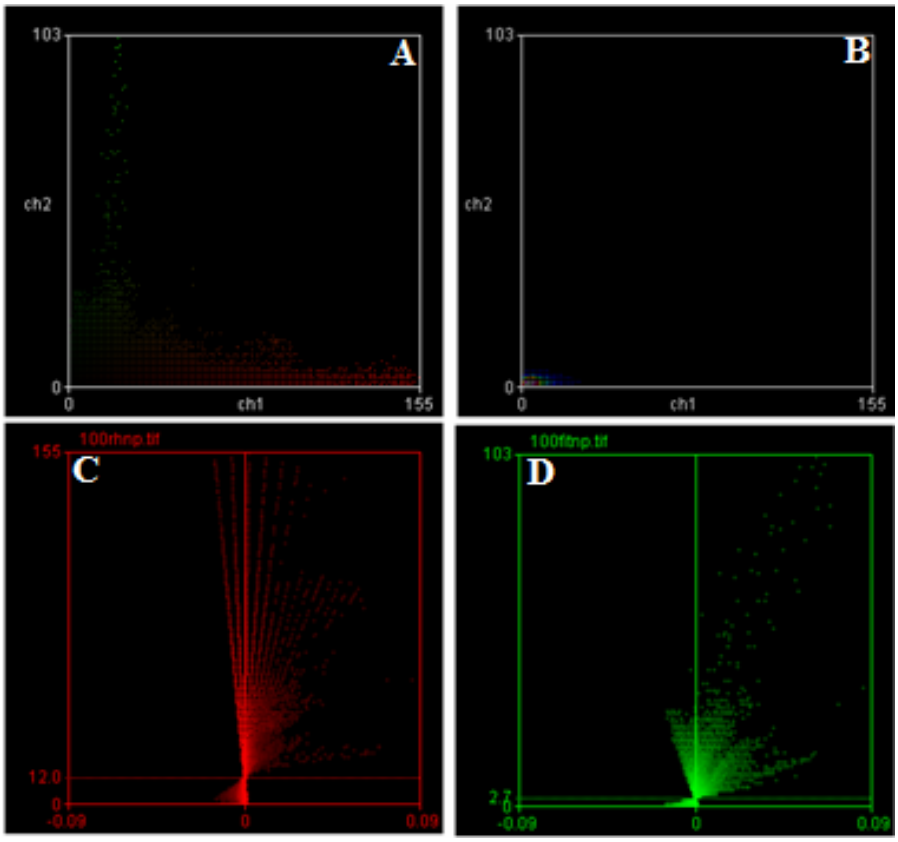


***Figure 23:*** *Colocalization analysis for the 1 µm control PDMS substrate showing the red-green scatter plot (A), the frequency scatter plot (B), the ICQ plots for the red (C) and green (D) channels. The scatter plots represent the intensity of the red pixels along the x-axis and intensity of the green pixels along the y-axis. The ICQ plots represent the product of the differences from the mean (PDM) on the x-axes while pixel intensities are represented on the y-axes.*

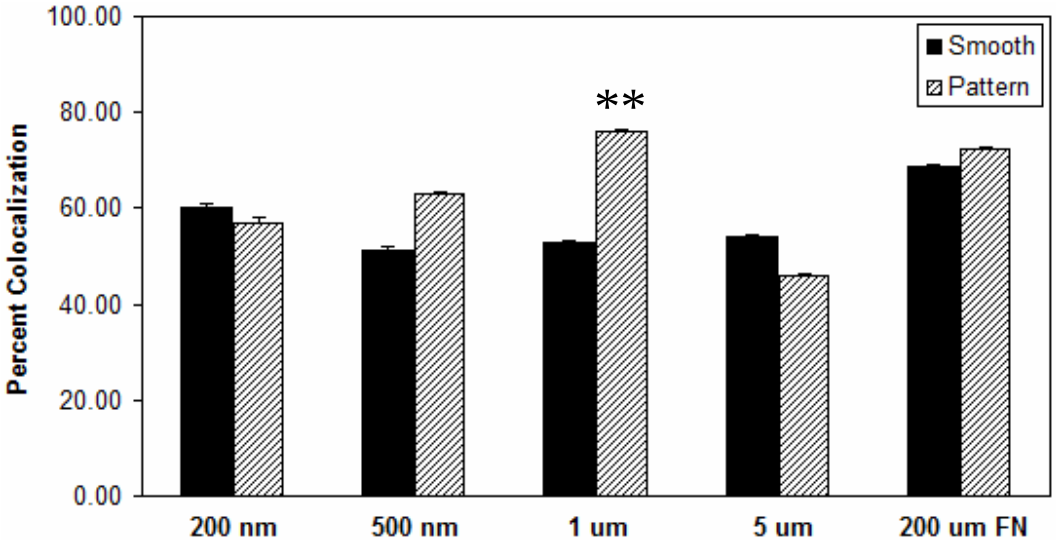


***Figure 24:*** *Histogram of the percentage of colocalization based on the Mander's Coefficient for the 200 nm, 500 nm, 1 µm and 5 µm groove depth patterns, as well as the 200 µm wide fibronectin pattern. The data are plotted as the mean ± standard deviation (SD). The ** above the 1 µm represents statistical significance at the 1% level ($p < 0.01$).*

From the histogram, it is seen that the percent colocalization increases from the 200 nm to the 1 µm groove depth, and a further increase in depth to 5 µm results in a significant decrease in the colocalization. The controls show minor differences in colocalization, which may be due to small variations in surface properties and/or in different confluent monolayers of BAECs. Clearly, the 1 µm groove depth shows the maximum colocalization, which along with the maximum cell alignment and elongation, makes this groove depth especially critical in inducing changes in confluent monolayers of endothelial cells. Further, comparing the 2D FN pattern to the groove patterns, it can be noted that the aligned and control sections of the FN pattern show higher levels of

colocalization as compared to the groove depths except the 1 µm. The 1 µm control sample is smaller than the control section of the FN pattern, while the aligned sample shows larger colocalization than the aligned section of the FN pattern. Although the microcontact printed FN patterns did not show changes in protein expression levels and distribution between control and aligned sections, it does exhibit fairly high levels of eNOS and Cav-1 colocalization that may be indicative of possible mechanisms involving these two signaling proteins with respect to 'sensing' of 2D surface geometries. Lastly, the colocalization data was tested for statistical significance. At the 5% level ($p < 0.05$), all differences between aligned (patterns) and control (smooth) experimental groups are statistically significant according to the Student's t-test. Also, the same statistical test was performed to compare the 1 µm depth colocalization to the other depths and the FN pattern, which confirmed that this depth had statistically higher colocalization at the 1% level of significance ($p < 0.01$).

### 4.5 Role of actin filaments in cell orientation

Following up on the interesting observation that BAECs on the 5 µm groove depth exhibited fluorescently labeled eNOS and Cav-1 aligning within the channels, cell cytoskeleton functions were thought to be involved. This experiment was designed to investigate the possible role of the cell cytoskeleton, specifically actin filaments, in cell orientation on grooved PDMS substrates by fluorescently labeling actin with a drug, phalloidin. Using fluorescence microscopy, the actin filaments of confluent monolayers

of BAECs on 200 nm, 500 nm, and 5 µm groove depth patterns were visualized (Figure 25).

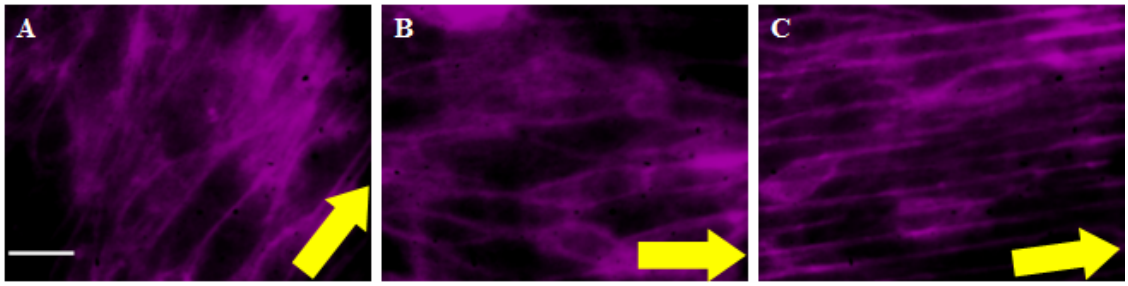


***Figure 25:*** *Fluorescent microscope images of actin filaments labeled using a drug, phalloidin, on the 200 nm (A), 500 nm (B), and 5 µm (C) groove depth PDMS patterns. The yellow arrows indicate the direction of the respective grooves, and the scale bar is 25 µm.*

Consistent with the results of the eNOS and Cav-1 staining, the actin filaments of the cytoskeleton are seen to align within the channels of the 5 µm groove depth, which is not the case for the 200 nm and 500 nm groove depths. Along with the actin filaments of the BAECs aligning within the channels, it is observed that the cell boundaries are aligning along the channels as well (Figure 25C). This may represent an interaction between Cav-1, eNOS and actin filaments of the BAECs cultured on the 5 µm groove depth, which allow these cells to 'sense' the underlying microtopography. To study a possible colocalization of these important signaling proteins with actin filaments, a triple staining fluorescent experiment was carried out (Figure 26). The results show that eNOS and Cav-

1 proteins align within the channels since they are fluorescently labeled in these images, as well as the actin filaments shown in the violet channel. A representative endothelial cell is identified by the small white arrow, which shows the eNOS protein distributed across the entire surface of the cell, the Cav-1 protein being localized at the ends of the elongated cell, and actin filaments that run through the cell boundary line up with the underlying 5 µm depth grooves.

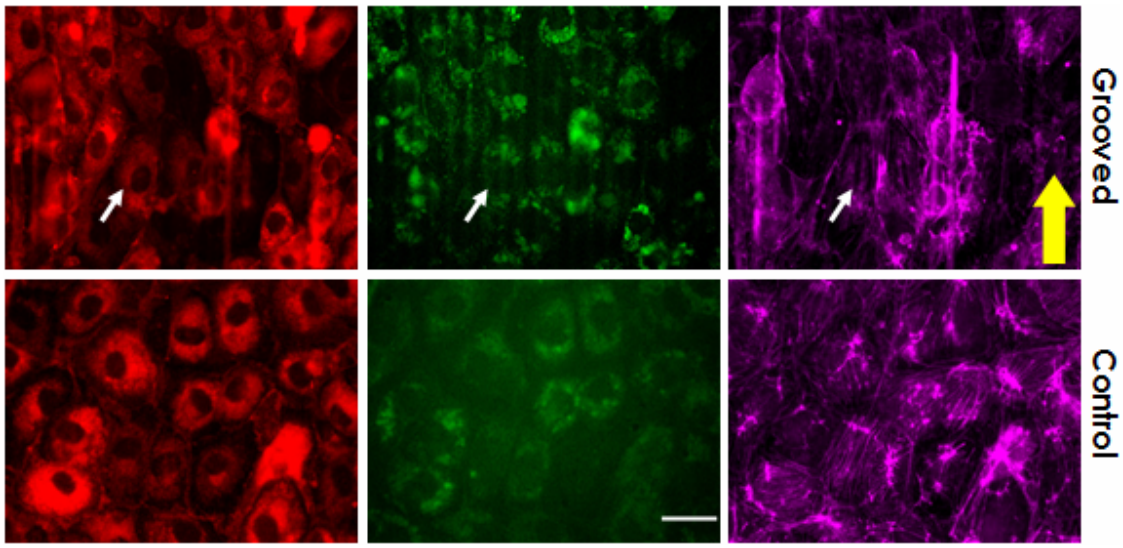


***Figure 26:*** *Fluorescent microscope images of BAECs cultured on a 5 µm groove depth PDMS pattern that have been triple stained for eNOS (red), Cav-1 (green), and actin (violet). The groove directions are represented by the yellow arrow. The smaller white arrows show an endothelial cell that clearly shows eNOS, Cav-1 and actin distribution. The scale bar is 25 µm.*

Based on these results, a mechanism by which endothelial cells 'sense' the underlying topography may involve eNOS, Cav-1 and actin filaments, as well as other components of the cell cytoskeleton. Further experimentation in addition to biochemistry-based techniques must be employed to accurately detail the signaling mechanism step-by-step, as well as gain a better understanding as to why the 5 µm groove depth is the only pattern that causes proteins and actin to align within the channels.

## 4.6 Discussion

Topographical cues have significant effects on cellular behavior. This study indicates that two-dimensional surface geometries and three-dimensional spatial arrangement of cells on nano- to micro-substratum have effects on the cells orientation and protein localization independent of one another. Here, we adopted poly(dimethylsiloxane) (PDMS) microgrooves to study the combined effects of 2D and 3D cues, and microcontact printing techniques using PDMS substrates to study the independent effects of 2D cues, on cell shape and protein distribution. A common effect of both 2D and 3D dimensions of the underlying substratum is that they affect bovine aortic endothelial cell (BAEC) morphology and orientation, which are results of altering the cell's microenvironment and eliciting local remodeling (Motlagh et al., 2003).

For the PDMS microgroove experiments, the variation in groove depth was hypothesized to provide endothelial cells with mechanical cues that would cause them to align and elongate along the direction of the grooves. This alignment and elongation is critical in

mimicking an in vivo environment, where a confluent, elongated endothelium is observed in the direction of blood flow (Nerem et al., 1981). According to this hypothesis, fluorescent microscopy images confirms that the BAEC alignment in the direction of the grooves increase with the increasing groove depth. This alignment (up to ~80% for the 1 µm depth) was visualized in confluent monolayers of endothelial cells rather than sub-confluent layers, which has been the standard in research investigations to date (Delft et al., 2008; Uttayarat et al., 2005). Further, the fluorescent labeling of Caveolin-1 and endothelial nitric oxide synthase (eNOS) showed that the cellular distribution of these proteins shift from being more cytoplasmic and peripheral randomly oriented cells to juxtanuclear in aligned and elongated endothelial cells. In addition, endothelial cells cultured on the 5 µm groove depth PDMS pattern showed Cav-1, eNOS and actin filaments aligning in the direction of the grooves, and in many cases localizing within individual channels. Similar results for actin filaments have been observed previously (Vartanian et al., 2008; Uttayarat et al., 2005). From these observations, it has been demonstrated that grooved nano- and micro-topography can successfully induce elongated endothelium in vitro in confluent monolayers.

Based on the PDMS microgroove experiments, it was hypothesized that the alignment of endothelial cells can be re-created using 2D patterns of the extracellular matrix protein, fibronectin. Developing microcontact printing procedures for fibronectin, 200 µm wide patterns were printed on smooth PDMS surfaces and cultured with endothelial cells, which resulted in randomly oriented cells in the mid section of the pattern while cells in the edge section of the pattern (50 – 80 µm) exhibited aligned and elongated cells parallel

to the direction of the protein boundary. This result is in agreement with prior studies (Vartanian et al., 2008). These results confirm that 2D surface cues are sufficient to create aligned and elongated layers of endothelial cells. In addition, fluorescent microscopy images of Cav-1 and eNOS in cells on these 2D fibronectin patterns showed cellular distribution was unchanged in the aligned cells as compared to the randomly oriented cells, specifically, Cav-1 was distributed across the cytoplasm and eNOS was localized juxtanuclear. This observation allows for the determination of the fact that PDMS microgrooves incorporate 3D cues, which are responsible for the differences in protein localization between aligned and non-aligned cells. This observation is comparable to results published by Hannachi et al. (2009). These microcontact printing patterns demonstrated successful isolation of the 2D cues responsible for cell shape changes that have been attributed to 3D parameters in several studies in the past that used microgroove patterned substrates.

# 5. CONCLUSION AND FUTURE WORK

## 5.1 Conclusion

The shape and protein expression of bovine aortic endothelial cells has been investigated on grooved poly(dimethylsiloxane) with variations in groove depth in the range of 200 nm to 5 µm and a fixed pitch of 8 µm, as well as 200 µm wide two-dimensional patterns of fibronectin. It has been shown that PDMS nano- and micro-grooves serves as an in vitro model to create confluent monolayers of endothelial cells that closely resemble vasculature. Further, surface microtopography is a useful technique for the study of shape-dependent properties of endothelial cells in the absence of fluid shear stress or other external forces. The 2D fibronectin patterns demonstrate the utility of microcontact printing techniques by confirming that the cell's response to underlying microtopography is a combination of the 2D surface geometry and the 3D spatial arrangement of cells. Based on the PDMS microgrooves and printed fibronectin patterns, it is reported that alignment of cells on 3D substrates (e.g. grooves) is what is responsible for variations in the distribution of important signaling proteins between aligned and randomly oriented cells. In terms of percent alignment and cell stretching, maximum alignment was observed to lie in the 500 nm – 1 µm groove depth range, with a maximum elongation on the 1 µm groove depth. Lastly, colocalization of Caveolin-1 and endothelial nitric oxide synthase (eNOS) may be related to the elongation of endothelial cells, because maximum elongation in cells resulted in maximum colocalization.

## 5.2 Future work

This study observed maximum cell alignment in the direction of the grooves on the 500 nm and the 1 µm groove depths respectively. The groove depth range of 500 nm – 1 µm should be further assessed in order to optimize the alignment of confluent layers of endothelial cells. Gaining a better understanding of the underlying mechanisms responsible for cell shape due to microtopography will require that the role of cell cytoskeletons, specifically actin filaments, in cell alignment and regulation of protein expression be studied. Furthermore, the effects of drugs being developed for cardiovascular diseases should be tested on aligned confluent monolayers of endothelial cells to evaluate its potential uses as an in vitro clinical model.

## LIST OF REFERENCES

Alberts, B., Johnson, A., Lewis, J., Raff, M., Roberts, K., & Walter, P. (2002) Molecular biology of the cell. *Garland Science*, 4th Edition.

Alexander, J.S., & Elrod, J.W. (2002) Extracellular matrix, junctional integrity, and matrix metalloproteinase interactions in endothelial permeability regulation. *J Anat*, 200, 561-574.

Andersson, A.S., Backhed, F., von Euler, A., Richter-Dahlfors, A., Sutherland, D., & Kasemo, B. (2003) Nanoscale features influence epithelial cell morphology and cytokine production. *Biomaterials*, 24(20), 2945-2954.

Ashkin, A., Dziedzic, J.M., & Yamane, T. (1987) Optical trapping and manipulation of single cells using infrared-laser beams. *Nature,* 330(6150), 769–771.

Baldwin, A.L., & Thurston, G. (2001) Mechanics of endothelial cell architecture and vascular permeability. *Crit Rev Biomed Eng*, 29, 247-278.

Britland, S., Morgan, H., Wojciak-Stothard, B., Riehle, M., Curtis, A., & Wilkinson, C. (1996) Synergistic and hierarchical adhesive and topographic guidance of BHK cells. *Experimental Cell Research*, 228, 313-325.

Cardena, G., Fan, R., Stern, D.F., Liu, J., Sessa, W.C. (1996) Endothelial nitric oxide synthase is regulated by tyrosine phosphorylation and interacts with Caveolin-1. *The Journal of Biological Chemistry*, 271(44), 27237-27240.

Carpenter, A.E., Jones, T.R., Lamprecht, M.R., Clarke, C., Kang, I.H., Friman, O., Guertin, D.A., Chang, J.H., Lindquist, R.A., Moffat, J., Golland, P., & Sabatini, D.M. (2006) CellProfiler: image analysis software for identifying and quantifying cell phenotypes. *Genome Biology*, 7, R100.

Chesmel, K.D., Clark, C., Brighton, C.T., & Black, J. (1995) Culture response to chemical and morphological aspects of biomaterial surfaces. II. The biosynthetic and

migratory response of bone cell populations. *Journal of Biomedical Materials Research*, 29, 1101-1110.

Chien, S., Li, S., & Shyy, Y.J. (1998) Effects of mechanical forces on signal transduction and gene expression in endothelial cells. *Hypertension*, 31, 162-169.

Choi, C.H., Hagvall, S.H., Wu, B.M., Dunn, J.C.Y., Beygui, R.E., & Kim, C. (2007) Cell interaction with three-dimensional sharp-tip nanotopography. *Biomaterials*, 28(9), 1672-1679.

Clark, P., Connolly, P., Curtis, A.S.G., Dow, J.A.T., & Wilkinson, C.D.W. (1990) Topographical control of cell behavior: II. Multiple grooved substrata. *Development*, 108, 635-644.

Cokakli, M., Erdal, E., Nart, D., Yilmaz, F., Sagol, O., Kilic, M., Karademir, S., & Atabey, N. (2009) Differential expression of Caveolin-1 in hepatocellular carcinoma: correlation with differentiation state, motility and invasion. *BMC Cancer*, 9(65).

Curtis, A., & Wilkinson, C. (2001) Nanotechniques and approaches in biotechnology. *Trends Biotechnol*, 19, 97-101.

Davies, P.F., Remuzzi, A., Gordon, E.J., Dewey, C.F., & Gimbrone, M.A. (1986) Turbulent fluid shear stress induces vascular endothelial cell turnover in vitro. *PNAS*, 83, 2114-2117.

Delft, F.C.M.J.M., Heuvel, F.C., Loesberg, W.A., Riet, J., Schon, P., Figdor, C.G., Speller, S., Loon, J.J.W.A., Walboomers, X.F., & Jansen, J.A. (2008) Manufacturing substrate nano-grooves for studying cell alignment and adhesion. *Microelectronic Engineering*, 85, 1362-1366.

Falconnet, D., Csucs, G., Grandin, H.M., & Textor, M. (2006) Surface engineering approaches to micropattern surfaces for cell-based assays. *Biomaterials*, 27(16), 3044-3063.

Fiorini, G.S., & Chiu, D.T. (2005) Disposable microfluidic devices: fabrication, function, and application. *BioTechniques*, 38(3), 429–446.

Flemming, R.G., Murphy, C.J., Abrams, G.A., Goodman, S.L., & Nealey, P.F. (1999) Effects of synthetic micro- and nano-structured surfaces on cell behavior. *Biomaterials*, 20(6), 573-588.

Folkman, J., & Moscona, A. (1978) Role of cell shape in growth control. *Nature*, 273, 345-349.

Frank, P.G., & Lisanti, M.P. (2006) Role of caveolin-1 in the regulation of the vascular shear stress response. *J Clin Invest.*, 116(5), 1222-1225.

Fry, D.L. (1968) Acute vascular endothelial changes associated with increased blood velocity gradients. *Circulation Res.*, 22, 165-197.

Gauvreau, V., & Laroche, G. (2005) Micropattern printing of adhesion, spreading, and migration peptides on poly(tetrafluoroethylene) films to promote endothelialization. *Bioconjugate Chemistry*, 16(5), 1088-1097.

Goessl, A., Garrison, M.D., Lhoest, J.B., & Hoffman, A.S. (2001) Plasma lithography—thin-film patterning of polymeric biomaterials by RF plasma polymerization I: Surface preparation and analysis. *Journal of Biomaterials Science, Polymer Edition*, 12(7), 721–738.

Hannachi, I.E., Itoga, K., Kumashiro, Y., Kobayashi, J., Yamato, M. & Okano T. (2009) Fabrication of transferable micropatterned-co-cultured cell sheets with microcontact printing. *Biomaterials*, 30, 5427-5432.

Head, B., Patel, H.H., Roth, D.M., Murray, F., Swaney, J.S., Niesman, I.R., Farquhar, M.G., & Insel, P.A. (2006) Microtubules and actin microfilaments regulate lipid raft/caveolae localization of adenylyl cyclase signaling components. *The Journal of Biological Chemistry*, 281(36), 26391-26399.

Herbert, C.B., McLernon, T.L., Hypolite, C.L., Adams, D.N., Pikus, L., Huang, C.C., Fields, G.B., Letourneau, P.C., Distefano, M.D., & Hu, W. (1997) Micropatterning gradients and controlling surface densities of photoactivatable biomolecules on self-assembled mono-layers of oligo(ethylene glycol) alkanethiolates. *Chemistry & Biology*, 4(10), 731–737.

Ji, Y., Ferraci, G., Warley, A., Ward, M., Leung, K., Samsuddin, S., Leveque, C., Queen, L., Reebye, V., Pal, P., Gkaliagkousi, E., Seager, M., & Ferro, A. (2007) Beta-actin regulates platelet nitric oxide synthase 3 activity through interaction with heat shock protein 90. *Proceedings of the National Academy of Sciences*, 104(21), 8839-8844.

Ju H., Zou R., Venema V.J., & Venema, R.C. (1997) Direct interaction of endothelial nitric-oxide synthase and Caveolin-1 inhibits synthase activity. *The Journal of Biological Chemistry*, 272(30), 18522-18525.

Kam, L., & Boxer, S.G. (2000) Cell adhesion to protein-micropatterned-supported lipid bilayer membranes. *Journal of Biomedical Materials Research Part A*, 55(4), 487-495.

Kato, S., Ando, J., & Matsuda, T. (2001) mRNA expression on shape-engineered endothelial cells: Adhesion molecules ICAM-1 and VCAM-1. *J Biomed Mater Res*, 54, 366-372.

Li, X., Everson, W.V., & Smart, E.J. (2005) Caveolae, Lipid Rafts, and Vascular Disease. *Trends in Cardiovascular Medicine*, 15(3), 92-96.

Lim, H.G., Cho, G.Y., Kim, J., & Kang, K.S. (2007) Au micro-pattern fabrication on cellulose paper: comparison of micro-contact printing and liftoff techniques. *Journal of Micromechanics and Microengineering*, 17(8), 1415-1419.

Malek, A.M., & Izumo, S. (1996) Mechanism of endothelial cell shape change and cytoskeletal remodeling in response to fluid shear stress. *J Cell Sci*, 109, 713-726.

Manders, E.E.M., Verbeek, F.J., & Aten, J.A. (1993) Measurement of co-localization of objects in dual-color confocal images. *Journal of Microscopy*, 169, 375-382.

Matsuzaka, K., Walboomers, F., de Ruijter, A., & Jansen, J.A. (2000) Effect of microgrooved poly-l-lactic (PLA) surfaces on proliferation, cytoskeletal organization, and mineralized matrix formation of rat bone marrow cells. *Clin. Oral Implants Res.*, 11, 325-333.

Michiels, C. (2003) Endothelial cell functions. *Journal of Cellular Physiology*, 196(3), 430-443.

Mokkapati, V.R.S.S., Piciu, O.M., Zhang, L., Mollinger, J., Bastemeijer, J., & Bossche, A. (2001) PDMS-glass bonded microfluidic device for single cell analysis: testing, alignment, bonding and trapping of polystyrene beads. *IEEE Conference Journal*, 415-419.

Motlagh, D., Senyo, S.E., Desai, T.A., & Russell, B. (2003) Microtextured substrata alter gene expression, protein localization and the shape of cardiac myocytes. *Biomaterials*, 24(14), 2463-2476.

Nerem, R.M., Levesque, M., & Cornhill, J. (1981) Vascular endothelial morphology as an indicator of the pattern of blood-flow. *J Biomech Eng*, 103, 172-176.

Noria, S., Xu, F., McCue, S., Jones, M., Gotlieb, A.I., & Langille, B.L. (2004) Assembly and reorientation of stress fibers drives morphological changes to endothelial cells exposed to shear stress. *Am. J. Pathol.*, 164, 1211-1223.

Oakley, C., & Brunette, D.M. (1993) The sequence of alignment of microtubules, focal contacts, and actin filaments in fibroblasts spreading on smooth and grooved titanium substrata. *Journal of Cell Science*, 106, 343-354.

Oakley, C., Jaeger, A.F., & Brunette, D.M. (1997) Sensitivity of fibroblasts and their cytoskeletons to substratum topographies: topographic guidance and topographic compensation by micromachined grooves of different dimensions. *Exp. Cell Res.*, 234, 413-424.

Palmer, R.M., Ferrige, A.G., & Moncada, S. (1987) Nitric oxide release accounts for the biological activity of endothelium-derived relaxing factor. *Nature*, 327, 524-526.

Pearson, J.D. (1999) Endothelial cell function and thrombosis. *Baillieres Best Pract Res Clin Haematol*, 12, 329-341.

Riveline, D., Zamir, E., Balaban, N.Q., Schwarz, U.S., Ishizaki, T., Narumiya, S., Kam, Z., Geiger, B., & Bershadsky, A.D. (2001) Focal contacts as mechanosensors: externally applied local mechanical force induces growth of focal contacts by an mDia1-dependent and ROCK-independent mechanism. *J. Cell Biol.*, 153, 1175-1186.

Scotchford, C.A., Ball, M., Winkelmann, M., Voros, J., Csucs, C., Brunette, D.M., Danuser, G., & Textor, M. (2003) Chemically patterned, metal–oxide-based surfaces produced by photolithographic techniques for studying protein- and cell-interactions. II: Protein adsorption and early cell interactions. *Biomaterials*, 24(7), 1147–1158.

Singhvi, R., Kumar, A., Lopez, G.P., & Stephanopoulos, G.N., Wang, D.I., Whitesides, G.M. & Ingber, D.E. (1994) Engineering cell shape and function. *Science*, 264(5159), 696-698.

Teixeira, A.I., Abrams, G.A., Murphy, C.J., & Nealey, P.F. (2003) Cell behavior on lithographically defined nanostructured substrates. *Journal of Vacuum Science and Technology Part B*, 21, 683-687.

Uttayarat, P. (2007) Chemical and physical modifications of silicone for novel vascular grafts. *Univ. of Pennsylvania - Electronic Dissertations.* Paper AAI3261000.

Uttayarat, P., Toworfe, G.K., Dietrich, F., Lelkes, P.I., & Composto, R.J. (2005) Topographic guidance of endothelial cells on silicone surfaces with micro- to nanogrooves: Orientation of actin filaments and focal adhesions. *Journal of Biomedical Materials Research Part B: Applied Biomaterials*, 75A(3), 668-680.

Vartanian, K.B., Kirkpatrick, S.J., Hanson, S.R., & Hinds, M.T. (2008) Endothelial cell cytoskeletal alignment independent of fluid shear stress on micropatterned surfaces. *Biochemical and Biophysical Research Communications*, 371(4), 787-792.

Walboomers, X.F., Croes, H.J., Ginsel, L.A., & Jansen, J.A. (1999) Growth behavior of fibroblasts on microgrooved polystyrene. *Biomaterials*, 19, 1861-1868.
Walboomers, X.F., Ginsel, L., & Jansen, J. (2000) Early spreading events of fibroblasts on microgrooved substrates. *J. Biomed Mater Res*, 51, 529-534.

Wehland, J., Osborn, M., & Weber, K. (1977) Phalloidin-induced actin polymerization in the cytoplasm of cultured cells interferes with cell locomotion and growth. *Proceedings of the National Academy of Sciences*, 74(12), 5613-5617.

Weiss, P. (1934) In vitro experiments on the factors determining the course of the outgrowing nerve fiber. *Journal of Experimental Zoology*, 69, 393-448.

Wojciak-Stothard, B., Curtis, A.S., Monaghan, W., McGrath, M., Sommer, I., & Wilkinson, C.D. (1995) Role of the cytoskeleton in the reaction of fibroblasts to multiple grooved substrata. *Cell Motil Cytoskeleton*, 31(2), 147-158.

Xiao, Z., Zhang, Z., Ranjan, V., & Diamond, S.L. (1997) Shear stress induction of the endothelial nitric oxide synthase gene is calcium-dependent but not calcium-activated. *J Cell Physiol*, 171, 205-211.

Yanagisawa, M., Kurihara, H., Kimura, S., Tomobe, Y., Kobayashi, M., Mitsui, Y., Yazaki, Y., Goto, K., & Masaki, T. (1988) A novel potent vasoconstrictor peptide produced by vascular endothelial cells. *Nature*, 332, 411-415.

Yim, E.K.F., Reano, R.M., Pang, S.W., Yee, A.F., Chen, C.S., & Leong, K.W. (2005) Nanopattern-induced changes in morphology and motility of smooth muscle cells. *Biomaterials*, 26, 5405-5413.

Zhu, B., Zhang, Q., Lu, Q., Xu, Y., Yin J., Hu, J., & Wang, Z. (2004) Nanotopographical guidance of C6 glioma cell alignment and oriented growth. *Biomaterials*, 25(18), 4215-4223.

Zhu, B., Lu, Q., Yin, J., Hu, J., & Wang, Z. (2004) Effects of laser-modified polystyrene substrate on CHO cell growth and alignment. *Journal of Biomedical Materials Research Part B: Applied Biomaterials*, 70B(1), 43-48.